Trust and Human Performance in Automated Formation Flight Station-keeping

by

Jinho Jang

Submitted to the Department of Aeronautics and Astronautics
in partial fulfillment of the requirements for the degree of

Master of Science in Aeronautics and Astronautics

at the

MASSACHUSETTS INSTITUTE OF TECHNOLOGY

August 2005

Author .....
Department of Aeronautics and Astronautics
August 20, 2005

Certified by .....
Mary (Missy) L. Cummings
Boeing Assistant Professor of Aeronautics and Astronautics
Thesis Supervisor

Accepted by .....
Jaime Peraire
Professor of Aeronautics and Astronautics
Chair, Committee on Graduate Students

Trust and Human Performance in Automated Formation Flight Station-keeping

by

Jinho Jang

Submitted to the Department of Aeronautics and Astronautics
on August 20, 2005, in partial fulfillment of the
requirements for the degree of
Master of Science in Aeronautics and Astronautics

Abstract

This thesis primarily describes performance and decision heuristics of human operators intervention with an autonomous formation flight (AFF) system during monitoring of a station-keeping display. Due to mental and physical workloads, automation technologies have been applied to formation flight for precise station-keeping and resultant fuel reduction, shifting control authority from humans to machines. Accordingly, the human is not directly in the control loop, but just supervises whether or not the automation works as intended. One critical problem in AFF supervisory control is that the human pilot needs to intervene with AFF system when the automated systems malfunction or their functions degrade. Thus while monitoring a station-keeping display, operators should minimize incorrect decisions for safety and cost reduction. To examine design issues in such a display, a simulation was constructed that simulated two different control systems as well as the impact of different angles of bank.

20 subjects participated in the monitoring task simulation of the station-keeping display. During the experiments, subjects were asked to intervene with AFF system when the AFF system failed to keep the trailing aircraft in the vortex area. Subjects made the most incorrect decisions when the AFF system was operated with the oscillating controller and high angle of bank. Trust of the human in the AFF system was found to be influenced by the damping ratio of the AFF controller. Most significantly, results showed that humans developed biased decision criteria to execute interventions because velocity feedback of the wing tip on this display was not adequately provided.

Thesis Supervisor: Mary (Missy) L. Cummings
Title: Boeing Assistant Professor of Aeronautics and Astronautics

Acknowledgments

I am deeply indebted to my research adviser, Missy Cummings, for her patient guidance and support for this thesis in the form of ideas, financial support, and moral support. She offered me the opportunity to carry out this research in the area that motivated me most. With a busy schedule, she has been always responsive and supportive to my requests, and always provided great ideas about my research. She has read each chapter with great care, often under extreme time pressure and made this thesis possible by her comments.

My sincere appreciation also goes to Greg Zacharias for being my second reader, and for his thorough readings and corrections. I am really grateful for the particular help of Kathleen Voelbel, Chris Tsonis and Paul Mitchell in preparing the experiments.

Great thanks to all the Humans and Automation Lab graduate students and research scientists who gave me helpful feedback on my interface and experimental designs: Stacey Scott, Paul Mitchell, Sylvain Bruni, Chris Tsonis, Angela Ho, Cristin Smith, and Jessica Marquez. I am also specially thankful to all subjects for participating in my experiment.

All my love and thanks to my wife, my daughter and parents for believing in me and supporting me. They has always encouraged me to try my best and to achieve what I have dreamed. Particularly, I would like to thank my dearest Sunwoo Kim for her love and understanding. I have to thank God for giving me the chance to study at MIT. I wouldn't have had this special chance without Him, and couldn't have made it without Him.

Contents

List of Figures

List of Tables

Chapter 1

Introduction

1.1 Motivation

1.1.1 Autonomous Formation Flight

For thousands of years, birds have realized aerodynamic benefits by flying in formation. Migratory birds such as Canadian geese fly in large formations, allowing the leading bird to create vortices in which the trailing (wingman) birds can reduce energy consumption. For example, great white pelicans appear to beat their wings less frequently and to glide for longer periods when flying in formation at optimal positions. The total energy savings that can be achieved is 11.4~14.0%, which is calculated from measuring the heart rate of the pelicans [28]. Figure 1-1 illustrates the V formation flight of migratory birds.

In a manner similar to migration birds, flying aircraft in formation can take advantage of the vortex created by the wing of the leading aircraft. An aircraft wing generates strong wing tip vortex, which causes an upwash field. By properly positioning a trailing aircraft within the vortices, aerodynamic benefit is achieved, especially for long-range missions. To reduce fuel expenditure in formation flight, aircraft should be positioned relatively close both laterally and longitudinally [2]. Scientists, using vortex lattice code HASC95, predicted a drag reduction of just over 20%. In attempt to verify theory, researchers examined how much benefit could be obtained through

Figure 1-1: Formation Flight of Birds [22]

station-keeping by a two-ship T-38 formation flight. Experimental results indicated a 15% drag reduction for the trail aircraft and an 11% fuel flow reduction. However, during the tests, it was discovered the maximum duration the pilots could keep the position was approximately 20~30 minutes [1], because manual formation flight increases physical and mental workload of pilots.

Autonomous formation flight testing (AFF) was recently completed at the National Aeronautics and Space Administration's (NASA) Dryden Flight Research Center. As opposed to the two T-38s test, two F–18 aircraft mounted with Global Positioning System (GPS) maintained the formation for 96 minutes with autopilot. Researchers measured drag reduction up to 20% for short intervals. The trail F–18 aircraft demonstrated a 12% fuel savings relative to the lead F–18 on the final test flight. It was also observed the pilots experienced high mental and physical workload increase even in the AFF[8, 27]. Figure 1-2 shows two F–18 aircraft in autonomous formation flight.

The implications and applications of AFF technology will be far reaching in the near future. With robust, precise, and safe AFF control systems, fuel economy ex-

NASA Dryden Flight Research Center Photo Collection
http://www.dfrc.nasa.gov/gallery/photo/index.html
NASA Photo: EC01-0328-3 Date: November 9, 2001 Photo by: Carla Thomas
Smoke generators show the twisting paths of wingtip vortices behind two NASA Dryden F/A-18 jets used in the Autonomous Formation Flight (AFF) program

Figure 1-2: Autonomous Formation Flight of Two F/A-18 Aircraft

tends to the domains of the cargo and passenger aircraft. In other future applications, such as aerial refueling, aircraft logistics, UAV swarming, and air traffic control, significant progress will be made with AFF technology.

1.1.2 Human Supervisory Issues in AFF

Machines are now carrying out many functions that have been performed only by humans: sensing variables, interpreting data, making decisions, and generating displays. Accordingly, the human is not directly in the control loop, but just supervises

whether or not the automation works as intended, which is known as human supervisory control. Human supervisory control (HSC) means that one or more human operators are intermittently programming and receiving information from a computer that interconnects through sensors and actuators to the controlled process or task environment [24]. The five roles for the supervisor are carried out during human supervisory control are illustrated in Figure 1-3. The supervisor begins with planning a task, and teaches the computer the planned task secondly. The third role is to activate and monitor the automation, and the fourth role is to intervene into the automation when required. Finally, the human learns from the experience and evaluates the performance. Figure 1-3 shows that the inner loop is activated when the supervisor intervenes in the automation, and the outer loop is activated when the supervisor learns from the experience and projects the learning to planning the next task [23].

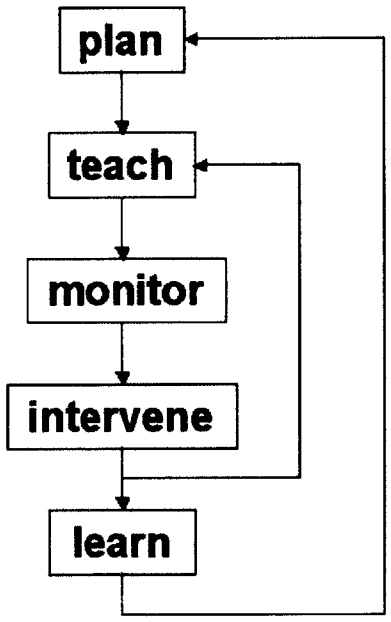

Figure 1-3: Five Roles of the Human Supervisor [24]

An automated system is thought to perform functions that have been performed

by humans more efficiently, reliably and accurately than a human operator. There is also the expectation that the automated machine can perform these functions at a lower cost than the human operator. Therefore, automated technology has advanced and become more prevalent, being applied at a rapid rate [17]. Failures and upsets of an automatic system, however, often lead to the catastrophic damage. Intervention by human operators occurs when failures or abnormalities occur in the automatic system, and the supervisor must interrupt the automation and manually take control. The question arises as to how and when the decision to intervene should be made by the human operator.

One of the technical challenges in keeping minimum drag formations is that the trailing aircraft cannot stay in a precise position. Since it is not possible for a pilot to fly manually in formation for long periods, it is generally accepted that the aircraft will require an AFF system to maximize the fuel savings and to fly safely. One crucial question in AFF research is to understand how a pilot functions as a human supervisor of the AFF control system. Employment of an automatic system deprives a human of control authority. However, a human is still responsible for monitoring the status of the automation even though the automatic system is in charge of station-keeping. The human supervisor generally intervenes when the computer does not carry out the designated goals, or when the state of the automation is abnormal [23].

Many researchers have attempted to design and develop AFF control algorithms and to implement AFF systems [15]. One challenge is how station-keeping displays should be designed to support pilot's monitoring of the AFF system. The AFF station-keeping display should provide the pilot with enough information to be aware of both current and future states of the system such that the pilot can judge if the automation is performing correctly. Without timely understanding of the current states, the pilot who is not actually flying the aircraft may not intervene with the AFF system correctly. As aircraft flying in formation is a high-risk environment, misunderstanding and extended time even for correct interventions could result in a catastrophe. However, AFF station-keeping may be less than fully perfect and reliable. The automatic system may not always operate in the intended way, so the

pilot might need to intervene. Thus, the key role of the station-keeping display is to send the pilot information concerning when the aircraft is in a dangerous position that requires intervention. Because the fundamental goal of AFF is to reduce energy expenditure, the station-keeping display should also minimize erroneous pilot interventions, which negates the benefit of the fuel savings. In addition to cost issues, once the pilot decides to intervene with the AFF system, the mental and physical workload highly increases as opposed to monitoring the display. The human does not rely on the automated system and the control authority shifts from the AFF system to the human pilot. The human pilot may control the formation flight temporarily before the AFF system corrects back to function normally or take control over the formation flight to the end of the given mission due to the irreversible failure of the AFF system.

One issue in monitoring AFF station-keeping is pilot's trust in the automation. Trust level of the human operator in the automation is a critical component of any HSC system with uncertainty, so understanding how the pilot's trust level is influenced in dynamic environments is considerably important [13]. Trust is considered a substantial factor in maximizing benefits obtained from the human-automation system. Previous studies revealed that the decision to perform the task manually or automatically depends upon the trust the human operators invest in the automation [12]. With low trust level in the automated system, the human operator is reluctant to use the automation and prevents the benefits from the automation. Excessive trust in the automated system causes the human operator complacent and to fail to intervene in the face of extreme situations.

There are a number of operational parameters that can affect the pilot's intervention performance such as a dynamic level of maneuverability and tight-tracking performance of the AFF controller. Trailing aircraft pilots develop a decision criterion for intervention depending on the relative position of the wing tip to the vortex area generated by the leading aircraft. For example, suppose that the leading aircraft in AFF entered a sharp turn. Then the vortices are created along the flight path of the leading aircraft, which influences the decision criteria to intervene because the vortex

area moves quickly following the motion of the leading aircraft.

1.2 Research Objectives

The research objective of this thesis in the context of human supervisory control is to investigate trust levels and performance of the human supervisor in the monitoring of AFF station-keeping. The first hypothesis in this research is that operational conditions have a significant effect on the intervening performance by human supervisor. The second hypothesis is that trust will be affected by operational conditions. In order to achieve these research goals, the display for station-keeping was designed based on dynamic simulation of the two-ship formation flight. This display was utilized for human experiments and data collected from the experiments were statistically analyzed.

1.3 Thesis Organization

This thesis is divided into six chapters. The chapter contents are summarized as follows:

- Chapter 1, *Introduction*, introduced research objectives and goals, and motivates the research effort.
- Chapter 2, *Background*, discusses previous works dealing with human interaction with automation and trust levels in the automation. It also describes the basic theory of formation flight and AFF control algorithms.
- Chapter 3, *Simulation and Display Design*, is devoted to the development of a simulation of formation flight and display design. Aerodynamic models, controller design, and formation system description are addressed.
- Chapter 4, *Experiments*, discusses experimental designs and tasks of the human subjects.

- Chapter 5, *Results*, presents the statistical analysis of data from the experiment described in the previous chapter.
- Chapter 6, *Discussion*, combines the results with the primary hypotheses and discusses the statistical analysis.
- Chapter 7, *Conclusion*, discusses the results and summarizes the thesis work. Based on these conclusions, the possible topic for future works are proposed.

Chapter 2

Background

This chapter presents the theoretical background on formation flight and explains the principle of the drag reduction. It then reviews the related works of AFF control systems and compares the different types of controllers that are used in formation flight. Finally, it provides the detailed discussion on trust in relation to automation and signal detection theory.

2.1 Basic Theory on Formation Flight

Wing-tip vortices form due to the difference in pressure between the upper and lower surfaces of a wing. The physical mechanism for generating lift on the wing is the combination of a high pressure on the bottom surface and a low pressure on the top surface. The net imbalance of pressure distribution generates the lift at a wing. However, as a byproduct of this pressure imbalance, the flow near the wing tips tends to roll up around the wing tips. These wing-tip vortices are counter-rotating and are essentially horizontal tornadoes that trail downstream of the finite wing. Eventually the tip vortices dissipate, their energy transformed by viscosity. The tip vortices produce additional downwash behind the wing within the wingspan. All the air within the wingspan has a tendency to move downward whereas all the air outside of the wingspan moves upward. Figure 2-1 illustrates the vortex flow produced by a jet airplane.

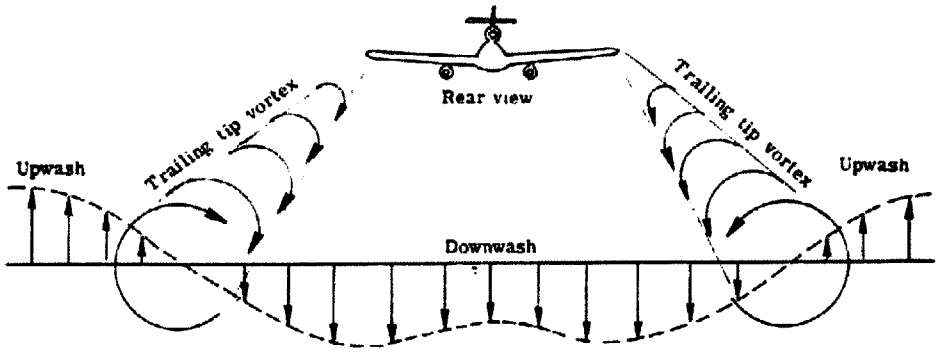

Figure 2-1: Wing tip vortex generated by a jet aircraft [22]

Drag reduction is obtained when the trailing aircraft is positioned in the upwash field generated by the leading aircraft [10]. Figure 2-2, adapted from Ray et al. [20], shows the rotation of the the lift (L) and drag (D) by the change in angle of attack ($\Delta\alpha$), which is due to the upwash (W) generated by the vortex. L' and D' represent the rotation of the original lift and drag. Two primary assumptions in this theory are that lift is greater than drag by an order of magnitude ($L \gg D$), and that the $\Delta\alpha$ value is small enough that $\sin(\Delta\alpha)$ can be approximated by $\Delta\alpha$ with high accuracy.

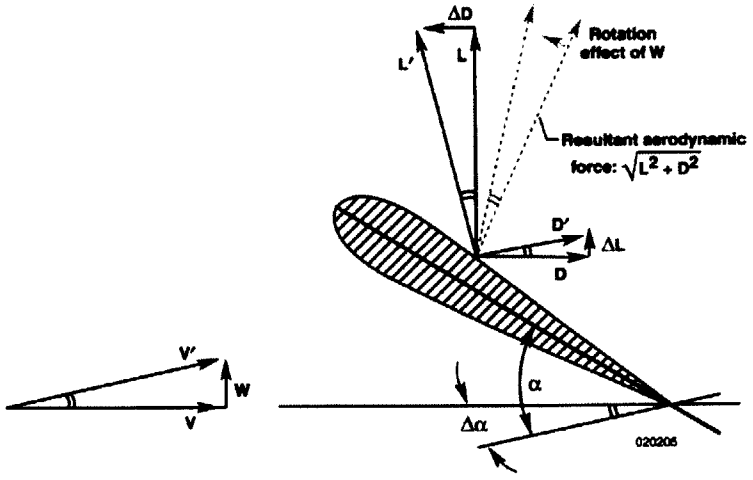

Figure 2-2: Rotation of resultant aerodynamic force caused by upwash [20]

This theory points out the magnitude of the resultant force ($\sqrt{L^2 + D^2}$) is constant

because the upwash just changes the direction of the force:

$$\sqrt{L^2 + D^2} = \sqrt{L'^2 + D'^2} \tag{2.1}$$

The term ΔD represents the drag change due to the rotation of the original lift force from L to L'. The total drag during formation flight, D_F, is represented as follows:

$$D_F = D' \cos(\Delta\alpha) - \Delta D \tag{2.2}$$

where

$$\Delta D = \sin(\Delta\alpha) L \tag{2.3}$$

Similarly, the term delta L represents the lift change due to the rotation of the drag force from D to D'. The total lift during formation flight, L_F, is represented as follows:

$$L_F = L' \cos(\Delta\alpha) + \Delta L \tag{2.4}$$

where

$$\Delta L = \sin(\Delta\alpha) D \tag{2.5}$$

Because lift is assumed to be an order of magnitude greater than drag ($L \gg D$), drag change becomes significantly greater than lift change:

$$\sin(\Delta\alpha) L \gg \sin(\Delta\alpha) D \tag{2.6}$$

$$\Delta D \gg \Delta L \tag{2.7}$$

Thus, considerable drag reduction can be attained by a small change in angle of attack, while lift is not significantly influenced. Reduced drag can yield lower fuel consumption since drag is proportionally related to fuel consumption. In reality, the upwash field outside of the wingspan does not simply rotate the aerodynamic forces of the trailing wing. However, the other effects of upwash are not considered because the rotation is the dominant effect [20].

2.2 AFF Control Algorithms

It is known that the trailing aircraft can benefit from drag reduction only when it is placed in a limited area of the vortex generated by its leading aircraft [2]. This area is called the sweet spot. However, it is also well known that efficient and collision-free formation flight requires highly accurate sensors, coordination protocols [6], and precise control systems. One of the main prerequisites for effective and safe missions is tight guidance and precise control of individual aircraft. This guidance and control algorithm should support a number of different tasks: formation initialization, formation contraction and expansion, coordinated turns, and pilot intervention.

Various automatic control algorithms have been developed to implement tight-tracking for drag reduction. The automatic control of the two-ship formation flight was considered [14], and this research resulted in the efficient design of proportional and integral (PI) controller that holds the lateral and longitudinal separation between the aircraft. In another study, close formation control where the lateral separation is less than wingspan was introduced with additional attention to the optimal formation-geometry for drag reduction [16]. A linear PI control law was employed and enabled the aircraft to take advantage of the reduction in the induced drag. In [14] and [16], the formation dynamics were confined to the horizontal plane and the aircraft were commanded to change the heading angle with a simple step function.

Other AFF control systems were further developed including full three-dimensional formation dynamics. A proportional, integral and derivative (PID) controller for the trailing aircraft was designed to maintain the specified formation despite the maneuver of the leading aircraft. Two candidate PID controllers were discussed and their performances were compared in three dimensions[7]. In [25], the author used the model of the relative distances dynamics to design a feedback-linearizing control system, but the model contains singular points. Recently, adaptive formation control algorithms were developed based on the body frames of the leading and trailing aircraft in the two-dimensional plane [3]. Nonlinear guidance algorithms also have been developed for tight tracking of curved paths and implemented with two UAVs [18].

If the desired trajectory is close to a straight line or a gentle curve then a simple control algorithms such as linear feedback controllers can provide acceptable performance [18]. The most common methodology in the linear feedback control is the PID controller. The PID controller receives signals from sensors and computes corrective action to the actuators from a computation based on the error (proportional), the sum of all previous errors (integral) and the rate of change of the error (derivative). A proportional controller is typically the main drive in a control loop and reduces a large part of the overall error. An integral controller reduces the final error in a system. Summing even a small error produces a drive signal large enough to move the system toward a smaller error. A derivative error helps reduce overshoot and damping. It has no effect on final error.

2.3 Signal Detection Theory

While the automated station-keeping will be expected to be reliable, it could fail or its function degraded, which leads to an extreme situation. Intervention into the AFF system by the human operator is required especially when the automated systems malfunction or their functions degrade. In addition to potential mechanical malfunctions, external environmental conditions, such as weather and any deviation from flight routines, also require quick human response. In this context, intervention is the last step taken by the human operator when the AFF system works improperly. Failure to understand those extreme situations and to interrupt the AFF system can result in disastrous consequences. When an extreme situation exists, the pilot can decide that the extreme situation is present or absent. These decisions are otherwise known as hits and misses respectively. Even if there is no extreme situation, the pilot can still decide that that the extreme situation is present or absent. These decisions are otherwise known as false alarms and correct rejections.

In the AFF system, intervention by the pilot has a disadvantage: the increase of the operating cost. The ultimate goal of the AFF is to reduce the operation cost by decreasing the fuel expenditure. The pilot cannot keep maximum drag formation flight

with manual control as precisely as the AFF system does. Manual formation flight diminishes the aerodynamic benefits attained by the AFF formation flight. Therefore, avoiding unnecessary interventions, which are defined by false alarms in this research, plays a vital role to decrease the overall cost of the AFF and becomes one of the reasonable measurements of the pilots intervention performance while monitoring the station-keeping display.

The terminology of hits, misses, false alarms, and correct rejections falls within the domain of signal detection theory (SDT). The basic assumption for SDT is that most decisions are made in the presence of some uncertainty. SDT provides a precise notation for analyzing decision making in the presence of uncertainty. SDT evolved from the development of communications and radar equipment during World War II. Then it moved to psychology in an attempt to understand some of the features of human behavior when humans make a decision, facing confusing stimuli. A classic radar is a typical example for SDT. When the radar detects an object, a radar operator makes a decision whether or not it is a signal of the enemy. However, other objects also cause similar signals, which makes the situation difficult. When the signal comes from the enemy, the radar operator can decide that it is either from the enemy or other objects. These outcomes are called hits and misses. If the signal comes from other objects, the operator can still decide that the signal is either from the enemy or other objects. These are called false alarms or correct rejections respectively. These outcomes are displayed in Figure 2-3.

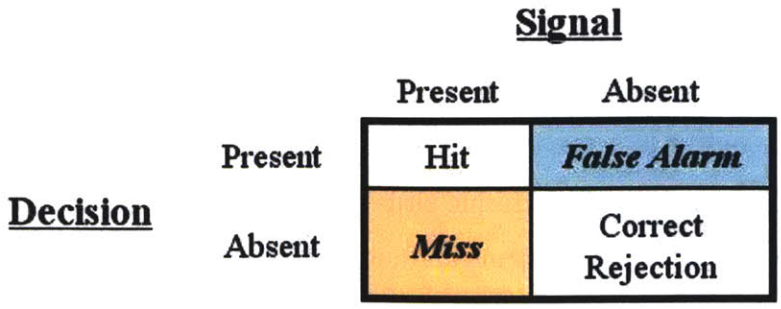

Figure 2-3: Signal Detection Theory

Figure 2-4 shows a graph of two hypothetical response curves. The left curve is the noise-alone probability density function, and the right curve is the signal-plus-noise distribution probability density function. It is assumed that the noise is normally distributed around the signal. The response for the signal-plus-noise is generally greater but the curves overlap, which means the response for a noise-alone trial may exceed the response for a signal-plus-noise trial.

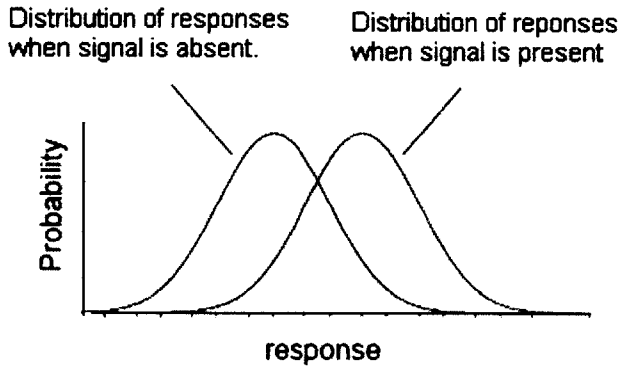

Figure 2-4: Probability density function for noise-alone and signal-plus-noise trials [9]

One of the main components to the decision-making process is a criterion. The simplest strategy that a human uses is to pick a criterion along the response axis. The vertical line in Figure 2-5 indicates a criterion. The criterion line divides the graph into four sections: hits, misses, false alarms, and correct rejections.

Thus, the human cannot always make correct decisions by manipulating the decision criterion. Suppose that humans choose a low criterion, so they very frequently respond at a slight signal that the signal is present. Then they will not miss the signal and they will have a high hit rate. However, responding at a slight signal will significantly increase the number of false alarms. If the subjects choose a high criterion, then they are unlikely to respond the signal is present even when the signal is real. They will not make false alarms, but they will also miss many real signals.

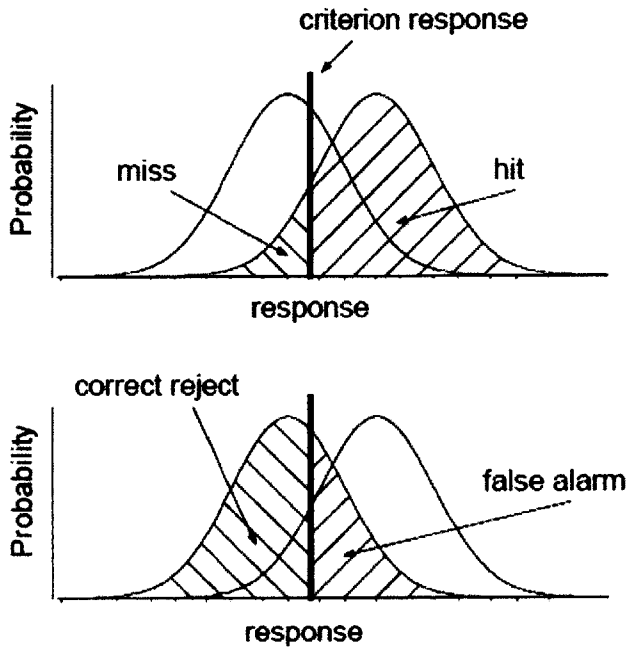

Figure 2-5: Criterion and outcomes: hits, misses, false alarm, and correct rejections [9]

2.4 Trust in Automation

Humans' trust in the automated system may influence the utilization of the automated system over manual control. The human operator who does not trust in an automated system may reject the use of the automation, no matter how intelligent it may be. If the human operators are forced to use the automation that they do not trust, it may be demanding and time consuming, and leads to degraded human performance. On the other hand, a human may trust the automation more than they should, allowing it to perform functions which can be performed better by a human or which may cause a system failure. Experiments conducted by Muir showed that decreases in trust corresponded to decreases in the use of the automated system [12]. However, Lee and Moray suggested that trust alone does not guide the percentage of time spent using the automatic control system [11]. Experiments conducted by Lee and Moray showed the operators' confidence in their manual control skills has a large influence

on choosing the manual control over the automatic controller.

Zuboff investigated the importance of trust in the relationship between operators and the systems with which they interact [29]. She documented operators' trust in the use of automation and her studies revealed two interesting phenomena. First, when the operators lack trust in a new technology, they often form a barrier, preventing the potential benefits that the new technology offered. Second, operators sometimes put excessive trust in the new technology, becoming complacent and failing to intervene when the technology failed.

In the human-machine systems, various machines have unequal predictability and reliability, and different functions of even a single machine do not necessarily have equal predictability and reliability. Therefore, it is infeasible for the human operator to trust or distrust them all equally. The human operator needs to adjust trust in machines, that is, to set trust to a level corresponding to trustworthiness of a machine or a function. Even though different machines show similar predictability, trust in machines will depend on the operator's mental models. Mental models are humans' views of a system that are formulated through interactions with the system. These models provide predictive and explanatory ability to understand both the system and interactions with the system [5].

Chapter 3

Simulation and Display Design

This chapter provides the details of a two-ship autonomous formation flight simulation and the design of the station-keeping monitoring display developed to study the effects of the operational conditions on human performance and trust in the automatic system.

3.1 Simulation

A two-ship formation flight was simulated on the basis of general aircraft dynamics, aerodynamics and automatic control. The basic model of the formation flight in this work is based on a Boeing 747 cargo airplane, which will be the most likely application of AFF in the commercial sector. The speed and altitude of both airplanes are assumed to be constant in order to simulate en-route conditions.

3.1.1 AFF Characteristics

Table 3.1 shows the formation flight characteristics in this work. Boeing 747 airplanes are flying in formation, where the trailing aircraft is behind the leading aircraft. They are keeping 500-meter downstream separation and flying at the altitude of 30,000 feet with the cruise speed 0.85 Mach (Figure 3-1). According to [2], the downstream separation should be between three and ten times of the wing span.

Basic Model	Two Boeing 747s
Cruise Speed	0.855 Mach
Altitude (h)	30,000 feet
Wingspan (b)	211 feet (64 meters)
Downstream Separation (d)	0.27 nautical mile (500 meters)
MAX. Angle of bank (AOB)	15°(Passenger) 25°(Cargo)

Table 3.1: Formation Flight Characteristics

Behind the leading aircraft, two vortex legs are shed and parallels by $(\pi/4)$b after the vortex is fully developed [26]. The automatic controller mounted on the trailing aircraft keeps the formation, maximizing drag reduction, by positioning the trailing aircraft safely in vortex. Seven wingspans are selected in this simulation. In the previous research of the fighter aircraft AFF, two F/A–18s were longitudinally separated by three wingspans [8], but due to the low maneuverability, a large aircraft requires more spacing to guarantee against a nose-to-tail crash.

3.1.2 Wing Tip Vortex and Drag Reduction

Aerodynamic drag is influenced by many factors such as wing shapes, size, and flow conditions. In the three-dimensional wing, there is an additional component of drag, called induced drag. This type of drag is created by the wing tip vortex and is a dominant drag component in high-lift wing such as Boeing 747. The ultimate goal of AFF is to reduce the induced drag of the trailing aircraft by properly positioning the trailing aircraft in the vortex, which results in the fuel savings. Total induced drag of a formation of two identical aircraft can be written as [19]:

$$C_{D_i} = \frac{{C_{L,1}}^2}{\pi AR} + \frac{{C_{L,2}}^2}{\pi AR} + \frac{2C_{L,1}C_{L,2}\sigma_1}{\pi AR} \tag{3.1}$$

The first two terms, which are fixed values, in Equation 3.1 represent the induced drag of leading and trailing aircraft respectively. These values depend on the aspect ratio and lift coefficient. The third term represents the mutual induced drag, which

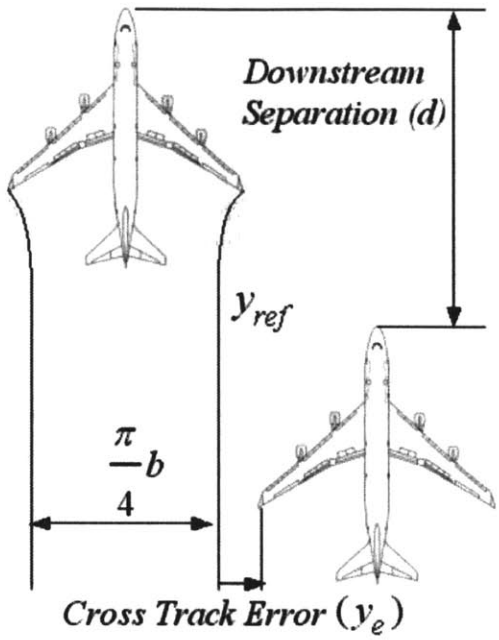

Figure 3-1: Formation Geometry

is given by coefficient of mutual induced drag, σ_1. A variety of aerodynamic methods can be used to compute the induced drag, and the horseshoe vortex model gives the term σ_1 as [19]:

$$\sigma_1 = \frac{1}{\pi^2}\left[\frac{\zeta^4 + 2\zeta^2\left(\eta^2 + (\pi/4)^2\right) + \left(\eta^2 - (\pi/4)^2\right)^2}{\left(\zeta^2 + \eta^2\right)^2}\right] \tag{3.2}$$

Spacing variables in Equation 3.2 are shown in Figure 3-2. Variables are non-dimensionalized by the wingspan. Equation 3.2 is graphically shown in the contour map in Figure 3-3. Positive values of σ_1 indicates the increase of the total induced drag and negative values of σ_1 indicates the decrease of the total induced drag. Figure 3-3 indicates that the maximum drag reduction is achieved when the wings are overlapped by 22% of the wingspan and two aircraft are co-planar. The area of maximum drag reduction area is very small, with a radius smaller than a tenth of a wingspan.

Drag reduction can be substantially attained when the wing tip of the trailing aircraft stays inside the contour where σ_1 is less than or equal to –0.12 [2]. Drag

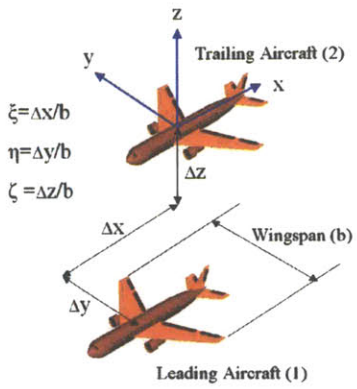

Figure 3-2: Formation Flight Geometry

increases or decreases slightly outside of this contour.

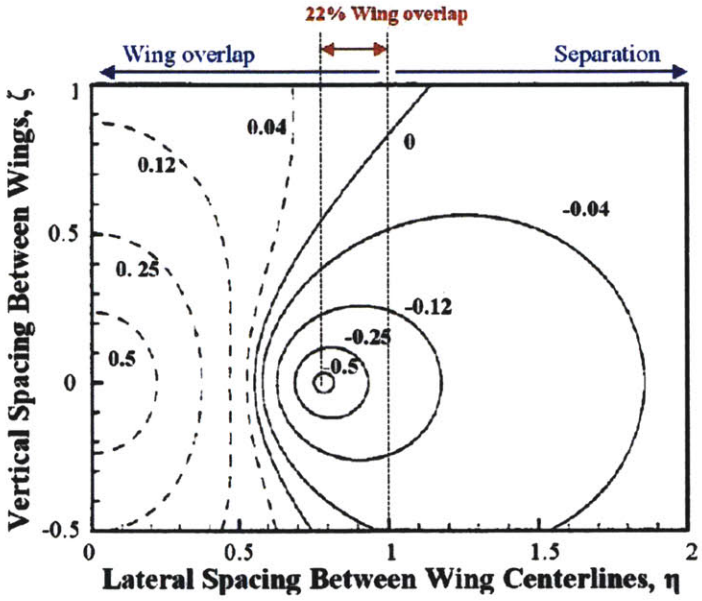

Figure 3-3: Variation of Mutual Induced Drag with Aircraft Position [2]

3.1.3 AFF Controller Design

The automatic controller is attached to the simulated trailing aircraft for station-keeping mission. The controller operates to keep the trailing aircraft inside the vortex area to reduce drag and to fly safely. The desired path for the wing tip of the trailing

aircraft is the right vortex leg (Figure 3-1) where drag reduction is maximized. The distance between the reference line, the right vortex leg, and the wing tip of the trailing aircraft is defined as cross track error or lateral error. This simulation starts with straight flight of a formation of two Boeing 747s, having no cross track error. When the two aircraft in formation turn without breaking the formation, the leading aircraft changes the heading angle. Then the automatic controller gives the command to the trailing aircraft to remove the nonzero cross track error. Lateral acceleration caused by angle of bank is used to correct the wing tip position back to the reference position. The basic dynamic model can be approximated to a double integrator because the position error is controlled by the acceleration. Figure 3-4 shows the rear view of the trailing aircraft and the vortex generated by the leading aircraft. The elliptic in Figure 3-4 represents the vortex area created by the leading Boeing 747 where σ_1 in Equation 3.1 is less than or equal to –0.12. The cross represents the wing tip position of the trailing aircraft. The dot is the vortex leg in Figure 3-2 where the induced drag is minimized. The major axis of the vortex area is estimated to 35.8m and the vortex leg from the right wing is shifted to the left from the center. In order for the wing tip to stay inside this area, the maximum overshoot to the left side should be less 10.6m, which is estimated by multiplying the lateral spacing in Figure 3-3 with the wing span of the Boeing 747.

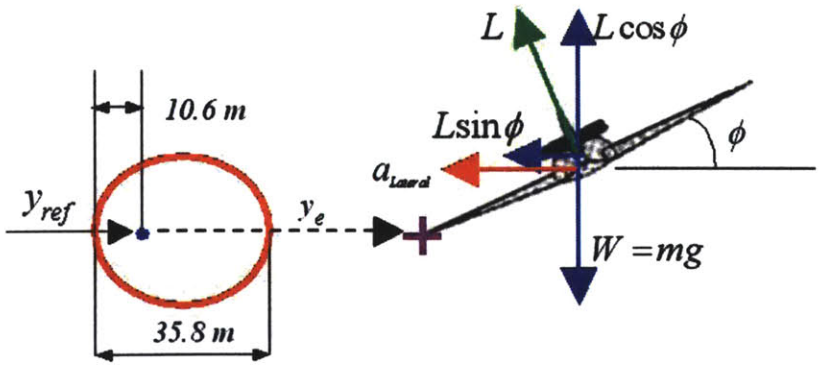

Figure 3-4: Vortex Area and Trailing Aircraft (Rear View)

As shown in Figure 3-4, the vertical component of the lift is identical to the weight

of the aircraft because it is assumed to be altitude-hold. The weight is assumed to be constant because the experiment (to be discussed in Chapter 4) only lasts for 20 minutes.

$$L\cos\phi = W = mg \tag{3.3}$$

Lift becomes as:

$$L = \frac{mg}{\cos\phi} \tag{3.4}$$

Lateral acceleration becomes by the Newton's Second Law as:

$$a_{Lateral} = \frac{L\sin\phi}{m} = \frac{mg}{\cos\phi} \times \frac{\sin\phi}{m} = g\tan\phi \tag{3.5}$$

The simple derivation of the lateral acceleration indicates the relation to the bank angle in Equation 3.5. To stabilize the formation flight system, a PID controller was implemented for the lateral channel as seen in Equation 3.6. k_d, k_p, and k_i represent the derivative, proportional, and integral controller gains respectively.

$$a_{Lateral} = -\left(k_d\dot{y}_e + k_p y_e + k_i\int_0^t y_e\,dx\right) \tag{3.6}$$

In order to detect the lateral error (y_e), a discrete step approach was taken. In the simulation of the AFF system, the time increment (Δt) was set to 100 milliseconds. Figure 3-5 shows the evolution of the detection logic in one time increment. In this diagram, reference points at each discrete time are marked by crosses on the reference line, which the wing tip of the trailing aircraft needs to track. At a certain instant of t_n, the first step was to find the first and second close reference points to the wing tip across the n reference points. Distances from the wing tip of the trailing aircraft to n reference points were measured and a bubble sort algorithm was used to find these two reference points. The first and second close reference points in this diagram were at t_k and t_{k+1}.

Then two vectors, which are $\vec{D}_{t_n}$ and $\vec{R}_{t_n}$, were defined from these two reference

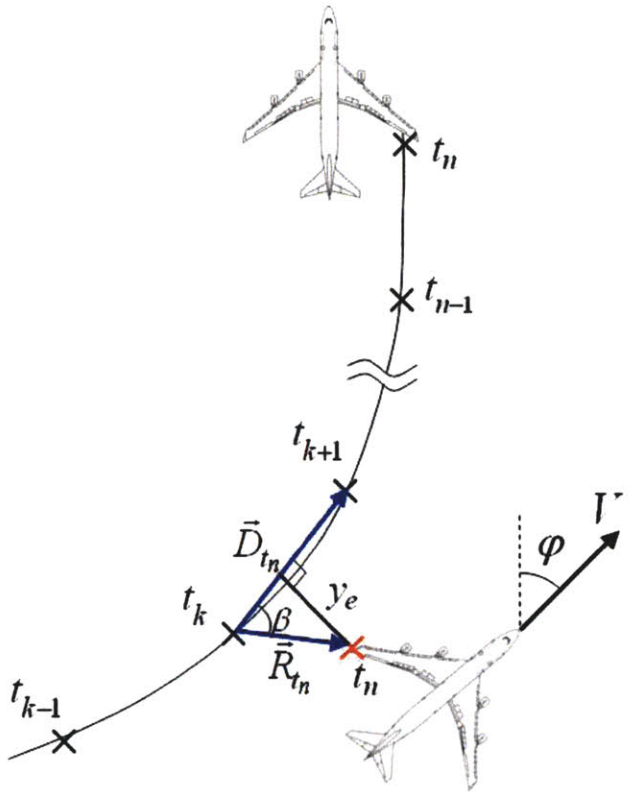

Figure 3-5: Discrete Representation: One Time Step

points and the position of the wing tip as seen in Figure 3-5. The magnitude of y_e became

$$|y_e| = \left|\vec{R}_{t_n}\right| \sin\beta \tag{3.7}$$

where

$$\sin\beta = \sqrt{1 - \left(\frac{\vec{D}_{t_n} \cdot \vec{R}_{t_n}}{\left|\vec{D}_{t_n}\right| \left|\vec{R}_{t_n}\right|}\right)^2} \tag{3.8}$$

The sign of y_e was negative when the wing tip of the trailing aircraft is to the left of the reference line. Finally, the lateral error was detected approximately as

$$
\begin{aligned}
y_e &= Sgn((\vec{D}_{t_n} \times \vec{R}_{t_n}) \cdot \vec{k})\, |y_e| \\
&= Sgn((\vec{D}_{t_n} \times \vec{R}_{t_n}) \cdot \vec{k}) \left|\vec{R}_{t_n}\right| \sqrt{1 - \left(\frac{\vec{D}_{t_n} \cdot \vec{R}_{t_n}}{\left|\vec{D}_{t_n}\right| \left|\vec{R}_{t_n}\right|} \right)^2}
\end{aligned}
$$

where $\vec{k}$ is a unit vector of the z-direction in Figure 3-2.

In a coordinated level turn, the heading angle (φ) is simply decided by the speed (V) and the angle of bank (ϕ). This relation became

$$
\int_0^t \frac{g \tan \phi(t)}{V}\, dt = \varphi(t) \tag{3.9}
$$

The mechanism of the guidance logic in this simulation is shown in Figure 3-6 with the discrete representation of Equation 3.9. According to the discrete time approach, the trailing aircraft translates by ΔS and rotates by $\Delta\varphi$ at each time step.

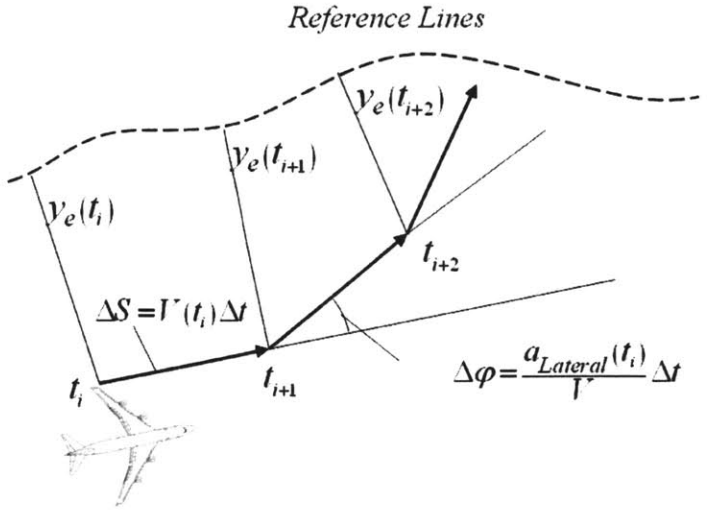

Figure 3-6: Discrete Representation of Trailing Aircraft Guidance Logic: One Time Step

The reference line is to the left of the wing tip of the trailing aircraft and the lateral error is a negative value. Therefore, at the next time step, the heading direction rotated counter-clockwise due to the lateral acceleration. The whole closed loop AFF

system in this simulation is the combination of the lateral error detection, the PID controller and the guidance logic, and the block diagram is shown in Figure 3-7.

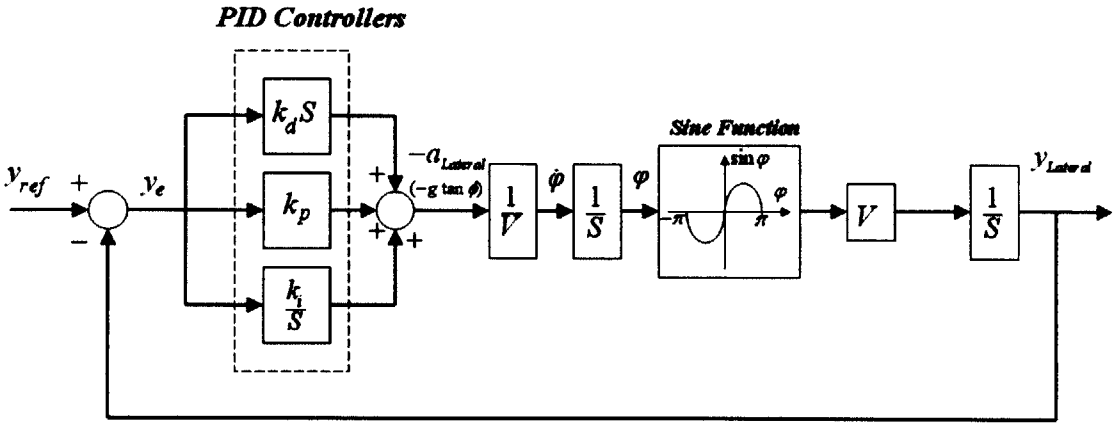

Figure 3-7: Block Digram of Dynamic Systems in the AFF

This closed loop includes the nonlinear element: a sine function. However, the perturbation of the heading angle (φ) at one time step is assumed to be small so that $\sin\varphi$ can be approximated to φ. Then the open loop transfer function of the AFF system became the double integrator (Figure 3-8).

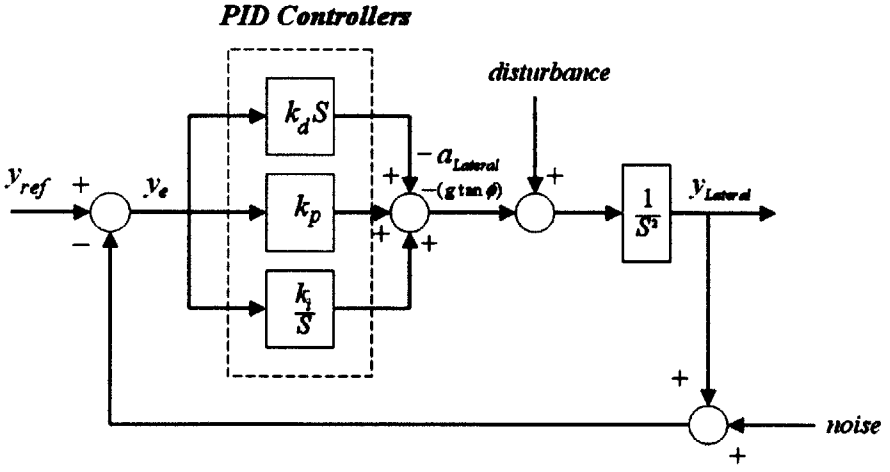

Figure 3-8: Simplified Block Diagram

In real formation flight, sensors, filters, and communication devices are included in the control loop to detect the relative positions of the aircraft without noise signals,

but this simulation is carried out computationally so it is assumed that two aircraft are able to detect the relative position and to estimate the vortex position to a great extent. The closed loop transfer function was derived from the above block diagram.

$$G_{CL}(s) = \frac{k_d s^2 + k_p s + k_i}{s^3 + k_d s^2 + k_p s + k_i} \tag{3.10}$$

3.2 Design of Station-keeping Display

Based on the AFF simulation, a station-keeping display was designed. C++ was used as the programming language. Open graphic library (OpenGL) and Microsoft foundation class (MFC) library were incorporated to support the graphical presentation of the simulation result. For a real-time simulation, a window timer was employed to set a time increment in the simulation as 100 milliseconds. This display would be mounted on the trailing aircraft and monitored by the pilot in the trailing aircraft. The display consisted of five components: vortex area generated by the leading aircraft, wing tip position of the trailing aircraft, warning signal, basic flight data, and static formation diagram. Figure 3-9 shows the AFF station-keeping display.

Figure 3-9: AFF Station-keeping Display

The vortex area is depicted as a three-dimensional tunnel in the display. The outer

most circle represents the area where the σ_1 is equal to –0.12 and drag is substantially reduced. The vortex tunnel moves following the flight motion of the leading aircraft. To design a three-dimensional display, a variety of effects are employed. Colors in the display were coded as an RGB image, which combines red, green, and blue color components for each individual pixel. In an RGB image of double type, the color values of red, blue, and green range from 0.0 to 1.0, 0.0 being the darkest and 1.0 being the brightest. Among the series of vortex circles, every fifth circle has a different color from the other four circles. The RGB array for every five circle was (1.0, 1.0, 0.0), while the other four circles had a RGB image of (1.0, 0.85, 0.0). As the aircraft fly forward, a series of vortex circles approaches toward the human operator. Differently colored circles generate the three-dimensional flow effect of the vortex tunnel. A perspective representation was supported by the color gradation.

Figure 3-10: Warning Signal Activation

The background is black because cargo airplanes usually fly at night, which represents instrument meteorological conditions. Conventional displays used at night require dark backgrounds to promote night vision. The white cross represents the

wing tip of the trailing aircraft, whose motion is controlled by the automatic system. In order to simulate the motions of the aircraft, a random function is added in the motion of the white cross that moves the cross slightly. Basic flight data are provided in the display: cruise speed, distance between the leading and trailing aircraft, angle of bank, and heading angle. When the white cross goes outside of the 80% of the vortex area, the warning signal above the vortex area is activated visually, changing from a brown "WARNING OFF" to a red "WARNING ON." Figure 3-10 shows the warning activation in the display. The warning signal was provided to notify the human operator that the wing tip approaches to the vortex boundary. However, warning activation does not necessarily mean the cross will go out and thus the wing tip of the trailing aircraft is no longer properly placed in the vortex. The goal of the warning system is to inform the human operator that the wing tip is close to the borderline of the vortex area. A static formation flight overview is displayed at the bottom left, which is the illustration of top view of formation flight.

Chapter 4

Experiments

The first part of this chapter presents the experimental procedures. The last part of this chapter provides the experimental design and participants.

4.1 Experimental Procedures

The subjects were instructed to monitor the station-keeping display as a trailing aircraft pilot in the AFF task. The trailing aircraft pilot is flying in a Boeing 747 cargo airplane at night time following the leading aircraft. The trailing aircraft pilot receives information of the vortex area and the wing tip's position only through the visual display. Each subject was given a practice scenario. Through the practice scenario, subjects recognized that a lateral error occured during the level turns and the AFF controller commanded corrective actions to the trailing aircraft.

The primary task was to make a decision to intervene with the AFF system in case of extreme situations. The ultimate goal of AFF is to guarantee safety and to maximize the fuel saving so the pilot should minimize the poor performance, as defined by false alarms and misses.

During test sessions, the leading aircraft deviated from the straight path to turn to the specified heading angle and the white cross, the wing tip of the trailing aircraft, sometimes approached to the borderline of the vortex area. During the transient response time, the corrective action by the PID controller, which included oscillation

and overshoot of the wing tip, caused the cross to be close to the boundary of the vortex area. The visual warning was then activated as mentioned in Chapter 3. The subjects were required to decide whether or not to interrupt the AFF system and take control. However, the warning activation did not necessarily mean the cross would go out. When the subjects decided to interrupt the AFF system, they pushed the space bar on the keyboard. Then the display stopped and the screen shot of the display was captured and saved. This screen shot informed relative position of the wing tip to the vortex area at the human's intervention. To continue the experiment, the subject pushed the shift key.

A secondary task was given to the subjects, which was observing the distance between the leading and trailing aircraft, because in the cockpit during an actual AFF mission, the pilot's attention cannot be entirely allocated to the AFF display. In order for the subject not to fixate on the cross position, the subject was asked to record on a sheet of paper when the nose-to-tail distance was less than 0.26 nautical miles.

4.2 Experimental Design

4.2.1 Independent Variables

Based on the AFF station-keeping display designed in Chapter 3, experiments on human subjects were designed and conducted. Two independent variables were used in this research: damping ratio of the AFF controller and limit of the bank angle command to leading aircraft. A human operator monitors whether or not the AFF system is working properly. Through the display, a human makes a decision to intervene the AFF system by watching the motions of vortex and wing tip position. When the cross, representing the wing tip of the trailing aircraft, fails to stay inside the vortex area, the pilot should interrupt the AFF system and take control over the aircraft. The pilot judges to intervene the AFF system from two sources - the motion of the vortex and the motion of the cross.

The vortex motion at level flight is primarily affected by the angle of bank because the vortex trails the wing tip of the leading aircraft. When the leading aircraft turns and heads toward a specified direction, the speed (V) and the angle of bank (ϕ) decide the heading angle (φ) in a coordinated turn (Equation 3.9). In contrast, the motion of the wing tip is affected by the controller of the AFF system. The AFF controller commands the trailing aircraft to keep the wing tip inside the vortex area by removing the cross track error. With a low damping ratio, the wing tip corrects back to the reference position with high oscillation. On the contrary, when the damping ratio is high, the wing tip moves smoothly without the oscillation. Therefore, it is hypothesized that two factors, the angle of bank and the damping ratio of the AFF controller, have a significant effect on human's intervention with the automation while monitoring the display.

In this study, both factors were designed to have two factor levels. When the leading aircraft entered level turning motions, two angles of bank, 15° and 25°, were commanded to the leading aircraft. These values were selected because typically, the bank angle should be less than 15° in passenger aircraft and 25° in cargo aircraft.

The lateral error of the wing tip position was corrected by the AFF controller with two different damping ratios, 0.1 and 0.7. From a controller-designing point of view, 0.7 is considered as a reasonable damping ratio [4]. The motion of the wing tip was oscillatory for a low damping ratio while for a high damping ratio, the motion showed no oscillation but became smooth. In the PID controller, a high derivative controller gain was required for 0.7 damping ratio. 0.1 damping ratio was selected for low damping because 0.1 damping ratio represents oscillation that can be visibly detected. The PID controller whose damping ratio was 0.1 should have relatively a high gain for an integral controller. When the trailing aircraft tracked the leading aircraft with 0.1 damping ratio, a pilot could observe oscillatory movement of the wing tip.

The two levels of damping ratio and two levels of angle of bank lead to 2×2 factor-level combinations. Two factors are fully crossed, i.e. all combinations of the levels of two factors are included in the study. Table 4.1 shows four factor levels. One

experimental scenario is designed for each factor level.

		Damping ratio	
		0.1	0.7
Angle of Bank (deg)	15	Scenario 1	Scenario 2
	25	Scenario 3	Scenario 4

Table 4.1: Factor Combination

The controller gains are calculated to meet the given damping ratio and the overshoot condition. Based on the wingspan of the Boeing 747 (64 meters), the overshoot of the wing tip from the desired path should be less than 10.6 meters in the context of drag reduction. PID controller gains are figured out by trial and error such that the wing tip stays marginally inside the vortex area at level turns unless turns have failure mode. Table 4.2 shows all PID controller gains, k_p, k_i and k_d.

	k_d	k_p	k_i
Scenario 1	2.861	1.296	2.338
Scenario 2	4.462	2.428	0.657
Scenario 3	3.107	1.992	3.856
Scenario 4	4.900	4.005	1.620

Table 4.2: PID Controller Gains

When the controller has low damping ratio (Scenario 1 and 3), the integral controller gain is relatively high in comparison with the proportional and derivative controller gains. On the contrary, the derivative controller gain is dominant with high damping ratio (Scenario 2 and 4).

As seen in Equation 3.10, the closed-loop transfer function had a third-order characteristic equation, which has one pole on the real axis and two complex conjugate poles as shown in Figure 4-1. The response of the AFF system is governed by two complex poles because the response by the real pole converges to the reference quickly.

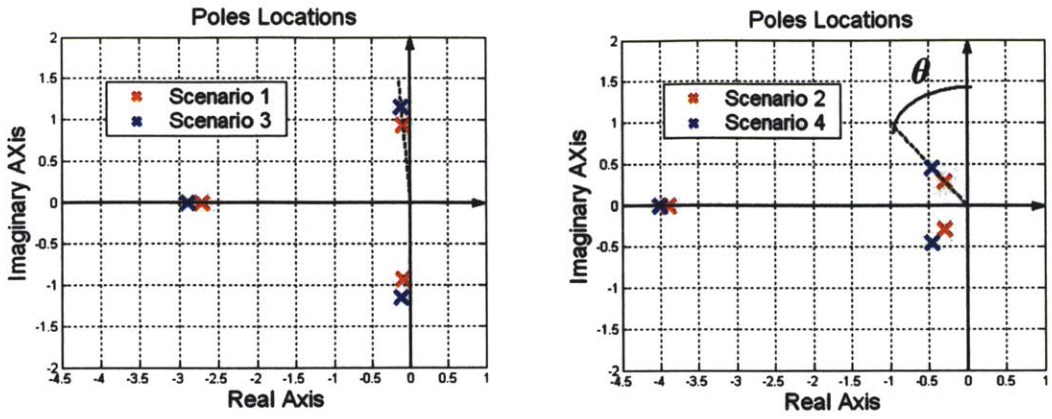

Figure 4-1: Location of Ploes (Left: Scenario 1 & 3, Right: Scenario 2 & 4)

The damping ratio (ζ) approximately becomes:

$$\zeta = \sin\theta \tag{4.1}$$

where θ is the deviation angle of the complex pole from the imaginary axis.

4.2.2 Dependent Variables

Three dependent variables were measured in this experiment: the intervention accuracy of the human operator, and the position and the velocity of the wing tip at the moment of intervention. While monitoring the station-keeping display, the pilot could make four types of decision based on the signal detection theory discussed in Chapter 2: hit, false alarm, miss and correct rejection. Among four decisions, misses and false alarms are grouped into the incorrect decision category. By analyzing the total number of incorrect decisions, misses and false alarms, the human's performance was measured. Secondly, the position and the velocity of the wing tip at the intervention were selected as dependent variables because investigation of these two variables will provide the human's decision criterion to intervene the AFF system.

4.2.3 Design of Experimental Scenarios

Each test scenario consists of eight level turns and six minutes are required to complete each scenario. Between turns, straight flight is inserted and the duration of straight flight is selected randomly between 17 and 23 seconds. The leading aircraft is commanded to fly to a specified heading angle in each scenario. When the angle of bank is limited to 15° (scenario 1 and 2), the heading angle is commanded to change 30°, 60° and 90° at each turn. On the contrary, when the leading aircraft banks up to 25° (scenario 3 and 4), the aircraft can change the heading angle by 60°, 120° and 180° at each turn.

Turn	Scenario 1	Scenario 2	Scenario 3	Scenario 4
1	30R	60L	60R	180L
2	30L	90R	120L	60R
3	90L	60L	180L	60R
4	60R	30L	180R	120L
5	30R	30R	60R	120R
6	90R	90L	120L	180R
7	60L	30R	120R	60L
8	60L	60R	60L	120L

Table 4.3: Turns in Scenarios and Failure Mode Turnings (Gray)

R and L in Table 4.3 represents right and left turns. In the experimental scenario design, orders of both heading angle changes and turning directions are randomized to prevent the ordering effect. Two out of eight turns have a failure mode. A failure mode indicates a malfunction of the AFF system where the white cross, the wing tip of the trailing aircraft, goes outside of the vortex area. Figure 4-2 shows the failure of the AFF system.

When the AFF system fails to control the wing tip to stay in the vortex region, the pilot has responsibility to intervene with the AFF system and takes control over

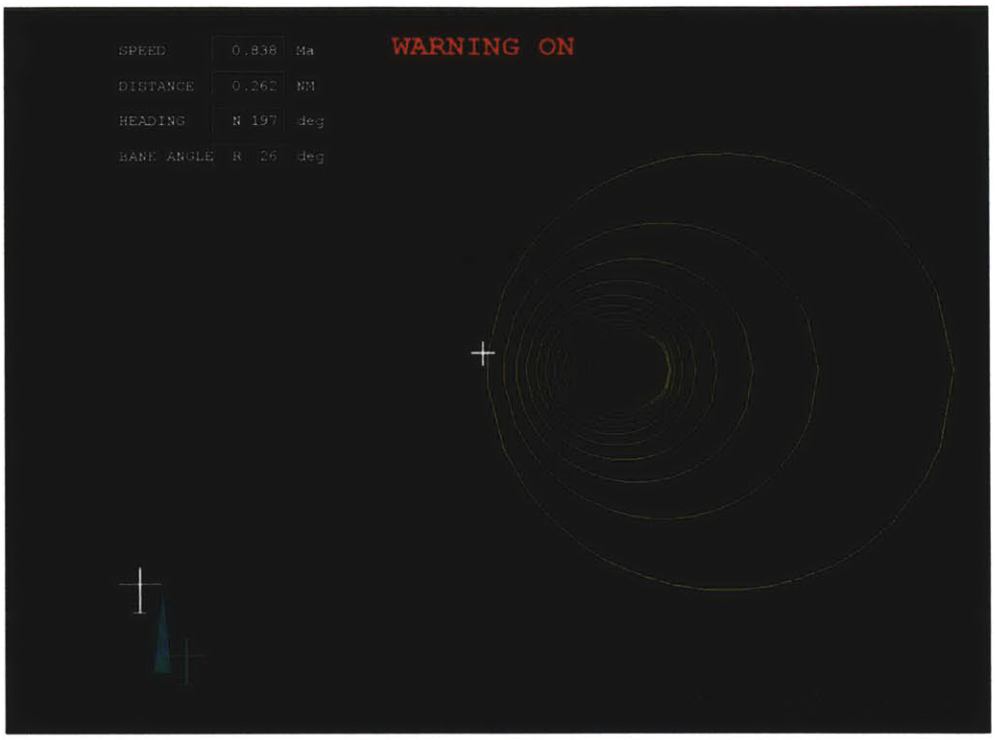

Figure 4-2: Failure Mode

the entire system for safety. Turns that have a failure mode are randomly distributed among eight turns in each scenario and are represented as the gray boxes in Table 4.3. To simulate failure of the AFF system, controller gains were dropped for specified turnings such that natural frequency of the closed-loop poles decreased to 80% of the original and had the same damping ratio.

From Equation 3.9, time required for the heading angle change is calculated with the given cruise speed. Times required for 30°, 60° and 90° heading angle changes in scenario 1 and 2 are approximately equal to those for 60°, 120° and 180° heading angle changes in scenario 3 and 4 (Table 4.4).

Before these four scenarios, one practice scenario is provided for subjects to be familiar with the display and the task. The practice scenario consists of 12 turns that are combination of three turns from each scenario, and takes around 10 minutes. Three failure modes are included in the practice scenario. Through this practice, subjects are able to experience all scenarios.

	Bank Angle(deg)	Time(sec)	Heading Angle Change(deg)
Scenario 1 & 2	15	8	30
		13	60
		18	90
Scenario 3 & 4	25	8.9	60
		14.5	120
		20.2	180

Table 4.4: Time Required for Heading Angle Change

4.3 Participants

A total of 20 participants participated in this experiment, 15 men and 5 women. The subject population consisted of undergraduates, graduates, and research scientists. All personnel were affiliated with MIT. $10 an hour were paid to all participants. The age of the subject population ranged from 21 to 31 with the average of 24.85 years.

Chapter 5

Results

This chapter provides the statistical results from the experiments described in Chapter 4. The first part of this chapter presents the human's intervention performance and the last part describes the position and the velocity of the wing tip at the moment of interventions. Intervention performance was evaluated by the counts of misses and false alarms.

5.1 Intervention Performance

As described previously in Chapter 4, the human's decisions are categorized into four decisions during the display-monitoring: hit, false alarm, miss and correct rejection. Each experimental scenario had eight turns and two turns out of eight turns had a failure mode. In the failure mode, the wing tip left the vortex area, which required intervention. When the AFF system did not work properly, the pilot performed a "hit" by interrupting the system correctly or a "miss" by failing to interrupt the system during a failure mode. In contrast, if there was no extreme situation and the pilot decided to interrupt the system, he/she performed a "false alarm", or if subjects did not interrupt the system, they performed a "correct rejection." By measuring the number of misses and false alarms, the performance of interventions can be analyzed. Table 5.1 represents the sum across all 20 subjects for the four decisions in each scenario.

	Scenario 1	Scenario 2	Scenario 3	Scenario 4
Hit	26	33	25	26
Miss	14	7	15	14
False Alarm	19	25	32	29
Correct Rejection	101	95	88	91

Table 5.1: Intervention Performance Data

As described in the previous chapter, tests consisted of four scenarios. Two independent variables, the angle of bank at turnings and the damping ratio of the AFF controller, were introduced. Table 5.2 shows the four experimental scenarios.

		Damping ratio	
		0.1	0.7
Angle of Bank (deg)	15	Scenario 1	Scenario 2
	25	Scenario 3	Scenario 4

Table 5.2: Factor Combination

5.1.1 Analysis of Missed Detections

The first performance metric examined was the number of misses for each AFF scenario, and as discussed previously, there were four scenarios that occurred in the random sequence. All the subjects were assigned to both the angle of bank and damping ratio factors. Figure 5-1 shows the sum across all 20 subjects for misses in each scenario.

Figure 5-1 demonstrates that the sum of misses performed by all subjects in scenario 2 is remarkably smaller than that in the other scenarios. To analyze the count of misses statistically, a Friedman test was used. The Friedman test is a non-parametric test for analyzing randomized complete block designs. The Friedman test specifics are included in Appendix A. The Friedman test showed that there is

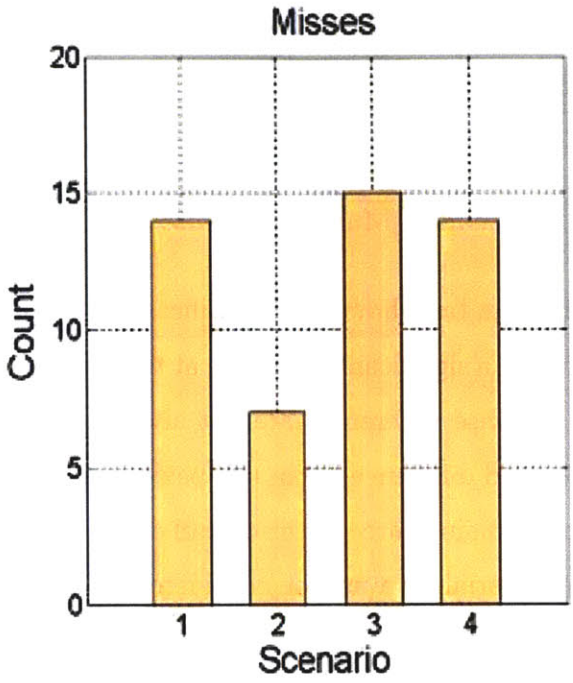

Figure 5-1: Sum of Misses

a significant difference between the factor levels ($\chi^2(3) = 9.111$, p = 0.028). In order to know where that difference lay, the significant difference of individual pairs of scenarios was examined, which is known as post-hoc pairwise comparisons. The Friedman pairwise test was used. The critical difference (D_{crit}) value in this test is given by the following formula when the significance level is 0.05 and 0.1, and the test is one-tailed:

$$D_{crit} = 2.394\sqrt{\frac{Nk(k+1)}{6}} \quad (\alpha = 0.05) \tag{5.1}$$

$$D_{crit} = 2.127\sqrt{\frac{Nk(k+1)}{6}} \quad (\alpha = 0.1) \tag{5.2}$$

where N is the total number of subjects in the experiment and k is the number of factor levels. If the observed difference between two rank totals is greater than the critical difference, then it is significant. Table 5.3 provides the critical difference at 0.05 and 0.1 significance level and the observed differences.

Critical Difference		Observed Difference			
α=0.05	α=0.1	1 vs 2	1 vs 3	2 vs 4	3 vs 4
19.55	17.35	14	2	14	2

Table 5.3: Friedman Multiple Pairwise Test in Misses

Even though the Friedman test showed the significant difference among the factor levels, there was no pair with a significant difference at the same level ($\alpha = 0.05$). This fact indicates that the pairwise differences are not always necessary for the overall difference. However, observed differences from two pairs, scenario 1 vs 2 and scenario 2 vs 4, were found to be the main source of the overall difference. Because interaction between two independent variables was not considered in the analysis, two pairs, scenario 2 vs 3 and scenario 1 vs 4, were not eligible for the pairwise comparison.

5.1.2 Analysis of False Alarm

In a similar manner, the number of false alarms in each scenario was examined. The Friedman test revealed that there is a significant difference in the sum of false alarms between the factor levels ($\chi^2(3) = 8.718$, p = 0.033). The sum of the false alarms for each scenario was depicted in Figure 5-2.

Figure 5-2 presents that subjects performed the most false alarms in scenario 3. The difference between the scenarios was primarily due to the difference between the scenario 1 and 3. Similarly, the Friedman pairwise test was used as a post-hoc comparison test. The critical difference is identical to that in the analysis of misses. Table 5.4 provides the critical difference and the observed differences. The observed difference between scenario 1 and 3 is significant when α is 0.1.

Critical Difference		Observed Difference			
α=0.05	α=0.1	1 vs 2	1 vs 3	2 vs 4	3 vs 4
19.55	17.35	11.5	19	4	2.5

Table 5.4: Friedman Multiple Pairwise Test in False Alarms

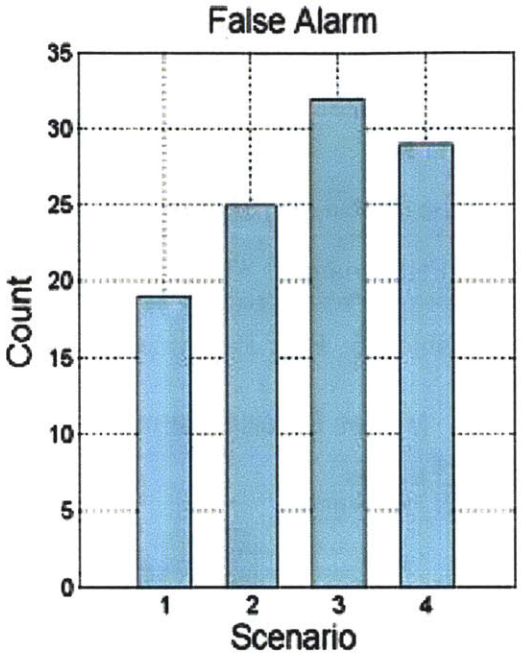

Figure 5-2: Sum of False Alarms

The reason we did not analyze hits and correct rejections is that the sum of hits and misses is constant in each scenario as well as the sum of false alarms and correct rejections.

5.1.3 Analysis of Poor Performance

Poor performance was previously defined as the incorrect decisions made by the human: misses and false alarms. It is critical to study the effect of the each factor on the poor performance in order to understand the human's general performance under the different operational conditions.

The poor performance measured in each scenario was calculated in Table 5.5 and graphically represented in Figure 5-3. According to the Friedman test, there is a significant difference between rank totals of the scenarios ($\chi^2(3) = 10.006$, p = 0.019). It graphically appears that the angle of bank has strong effects on the poor performance in the intervention with the AFF system because the number of poor performances in scenario 3 and 4 was remarkably greater than that in scenario 1 and

	Scenario			
	1	2	3	4
Miss	14	7	15	14
False Alarm	19	25	32	29
Poor Performance	33	32	47	43

Table 5.5: Poor Performance

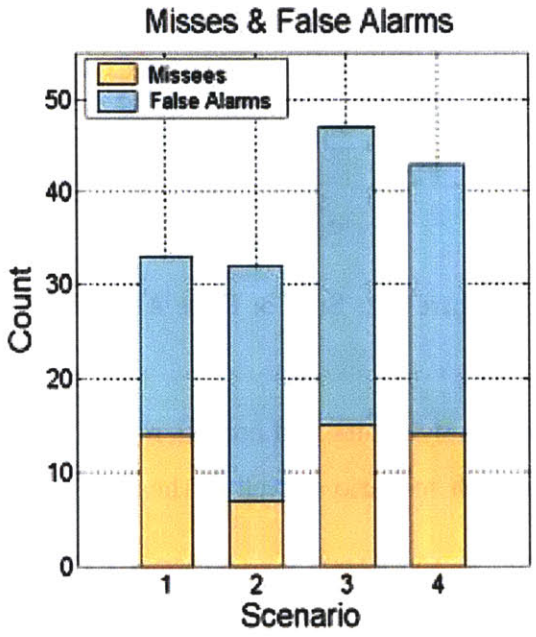

Figure 5-3: Sum of Poor Performance

2. Similarly, the Friedman pairwise test was carried out to find out the main sources of the difference between rank totals of the scenarios (Table 5.6).

As shown in Table 5.6, the observed differences in rank totals from individual pairs were small when the AFF was operated at 15° angle of bank. However, the differences in rank totals increased as the angle of bank changed from 15° and 25°. At sharp level turns generated by the high angle of bank, the human's performance degraded and incorrect decisions increased. In addition to this result, the fewest poor performances occurred when the smoothing controller was provided and the angle of

Critical Difference		Observed Difference			
α=0.05	α=0.1	1 vs 2	1 vs 3	2 vs 4	3 vs 4
19.55	17.35	0	17.5	13.5	5

Table 5.6: Friedman Multiple Pairwise Test in Poor Performances

bank was limited to 15° at the level turn. On the contrary, the combination of the oscillation controller and 25° angle of bank caused the greatest poor performances.

Both the graphical depiction and pairwise comparisons suggest that the angle of bank influenced the overall poor performance so Wilcoxon-Signed Rank test was used to examine that effect (Appendix A). This test demonstrated that there is a significant difference in counts of poor performances between two bank angles (z=–2.956, p=0.003). Figure 5-4 shows sum of the poor performances at each angle of bank. As the angle of bank increases, both misses and false alarms increase.

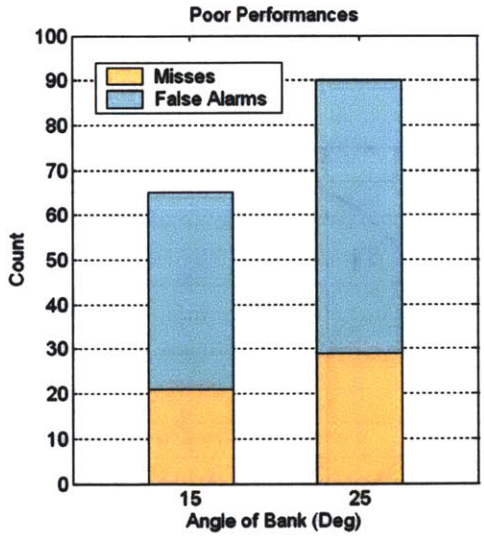

Figure 5-4: Poor Performances of each angle of bank

5.2 Positions of the Wing Tip at Interventions

Because the previous analysis just considers the counts of incorrect performances, the basic nature of human decision rules were not involved. In order to understand what decision rules the human generated and how the human developed these rules, the positions and velocities of the cross were investigated. Humans make decisions through the display based on position and time derivatives of positions. Therefore, to investigate the decision threshold at the moment of intervention, the positions of the wing tips were analyzed first.

To quantify the positions of the wing tip at interventions, the radial distance of the wing tip from the origin was measured from the screen shot of the display. The wing tip and vortex area at the screen shot were mapped onto the non-dimensionalized domain by the wing span. In Figure 5-5, the origin indicates where the maximum drag reduction occured based on the horseshoe vortex model [19]. $R2$ is the distance from the origin to the cross while $R1$ indicates the distance from the origin to the vortex area boundary in the radial direction of the cross. The ratio of these two radial distances, which is $R2/R1 \times 100\%$, was employed as a dependent variable in this experiment. This dependent variable is illustrated in the Figure 5-5.

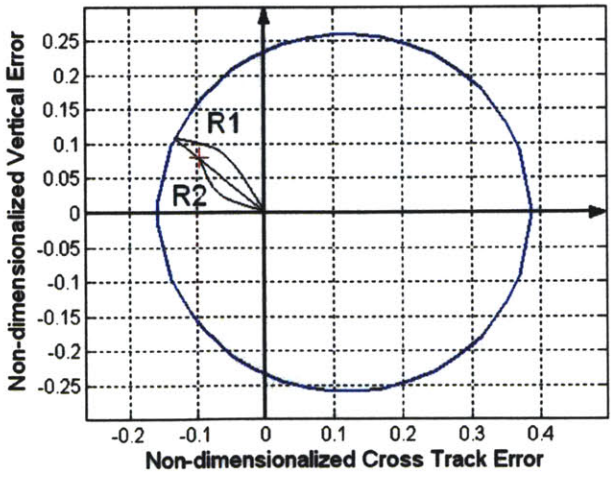

Figure 5-5: Percentage of the Distance of the Wing Tip Position

Figure 5-6 shows how far from the origin the cross was when subjects intervened with the AFF system in hits and Figure 5-7 in false alarms.

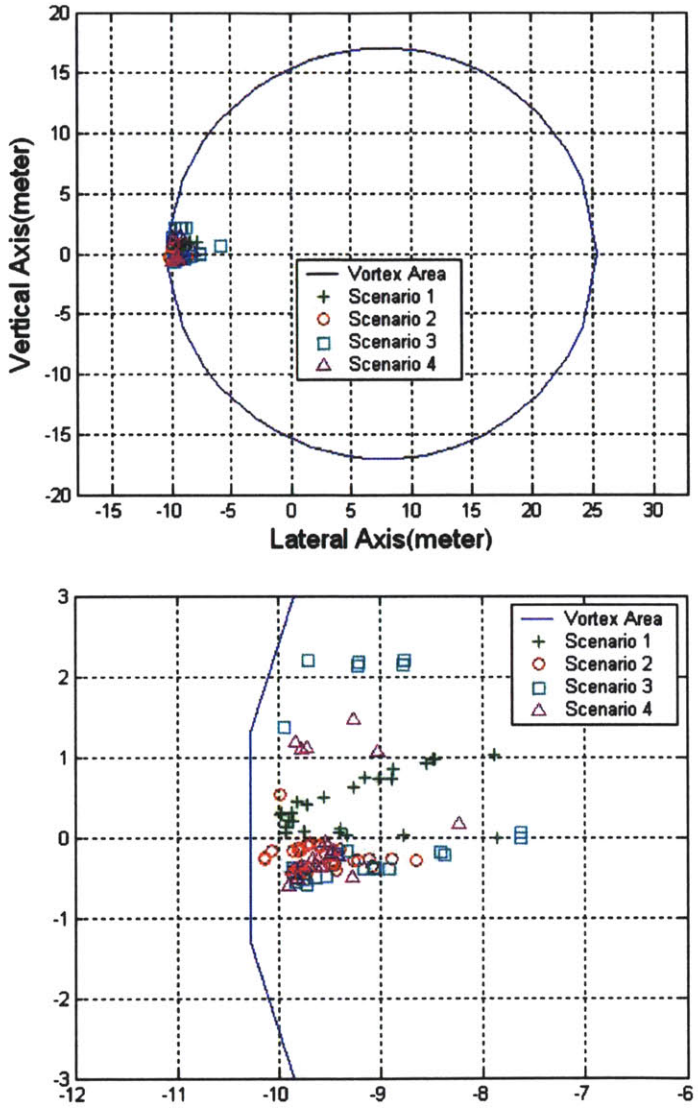

Figure 5-6: Positions of the wing tips at hits (Top) and zoom-in view (Bottom)

All interventions occurred at the left side in both hits and false alarms. Because the AFF system turns were level, the vertical error was not considered. Mean percentage of radial distances bewteen hits and fale alarms was compared, which resulted in no significant difference at intervention positions between correct and incorrect

interventions (z = 0.7560, p = 0.225).

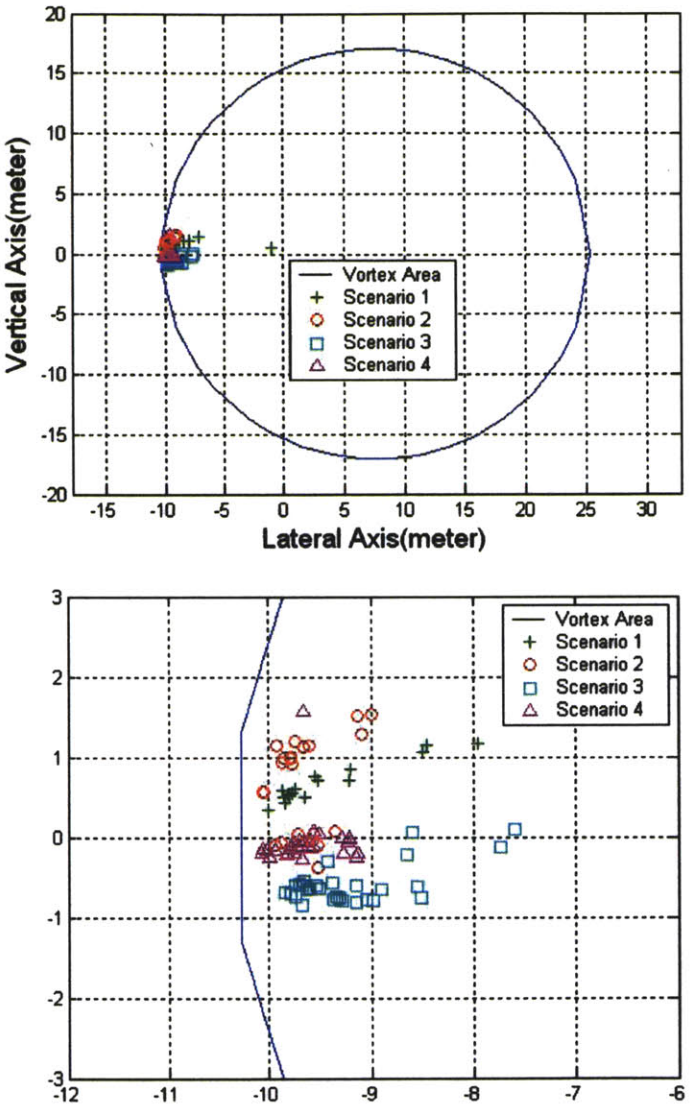

Figure 5-7: Positions of the wing tips at false alarms (Top) and zoom-in view (Bottom)

Two factor 2×2 ANOVA (Analysis of Variance) test was conducted on the percentage of the radial distance for both hits and false alarms. As previously mentioned, it was assumed that the distance of the wing tip from the origin was influenced by the two factors, which were the angle of bank and the damping ratio of the AFF controller. Both factors were designed to have two factor levels. The main interest was to

examine what factors have a significant effect on the human's intervention positions. In regards to hits, of the main effect, only the damping ratio of the AFF controller was found to be highly significant ($F(1,106)=16.620$, $p<0.001$). However, the angle of bank and the interaction between two factors had no significance. In the falses alarms analysis, the damping ratio of the AFF controller was also only significant of the main effects ($F(1,100)=17.011$, $p<0.001$).

5.3 Velocities of the Wing Tip at Interventions

By monitoring the display, the human operator obtained both positional information and velocities of the wing tip. The following figures show the lateral error of the wing tip from the origin at the time domain. In Figure 5-8, the lateral error of the wing tip is plotted on the time domain, and the positions of hits and false alarms are marked when aircraft banked to 15° and underwent 30°, 60°, and 90°. In Figure 5-9, interventions at scenario 3 and 4 are presented.

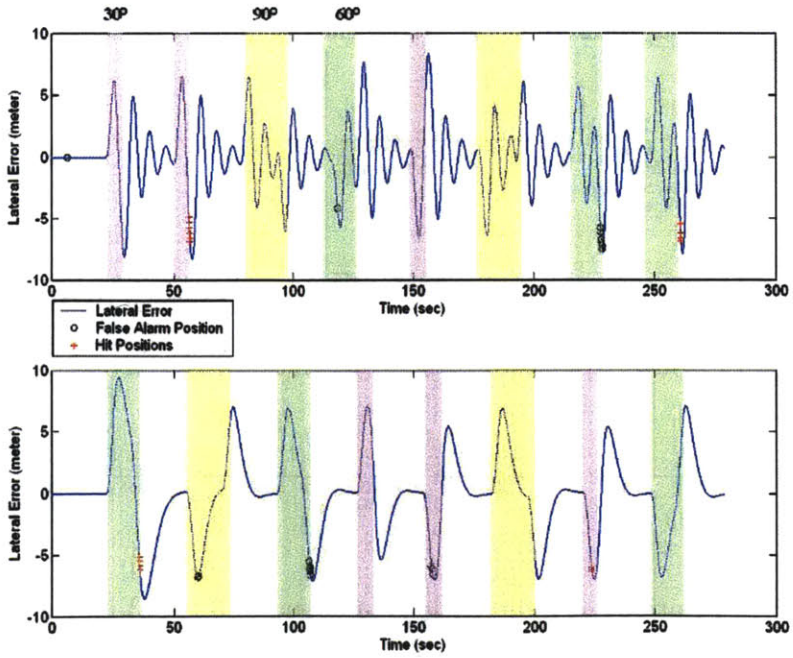

Figure 5-8: Positions of Interventions in Scenario 1 (Top) and 2 (Bottom)

The shaded area with different colors specified the AFF heading angle change corresponding to those colors. When the aircraft banked to 15° in scenario 1 and 2, the shaded time intervals with red, green and yellow represent 30°, 60° and 90° heading changes. In scenario 3 and 4, 60°, 120° and 180° heading changes occurred during the the shaded time intervals with red, green and yellow.

The cross (+) and the circle (o) represent hits and false alarms respectively. Velocities of the wing tip at interventions are the first time-derivative of the position so they can be derived from these plots. Graphically, the slope at the time domain represents the velocity at that point. For every intervention, the numerical differentiation method was used to find the velocity. These velocities of the wing tip were depicted together with positions of interventions for both hits and false alarms. The magnitude and the direction of arrows in Figure 5-10 show the velocity vector of the wing tip at that position.

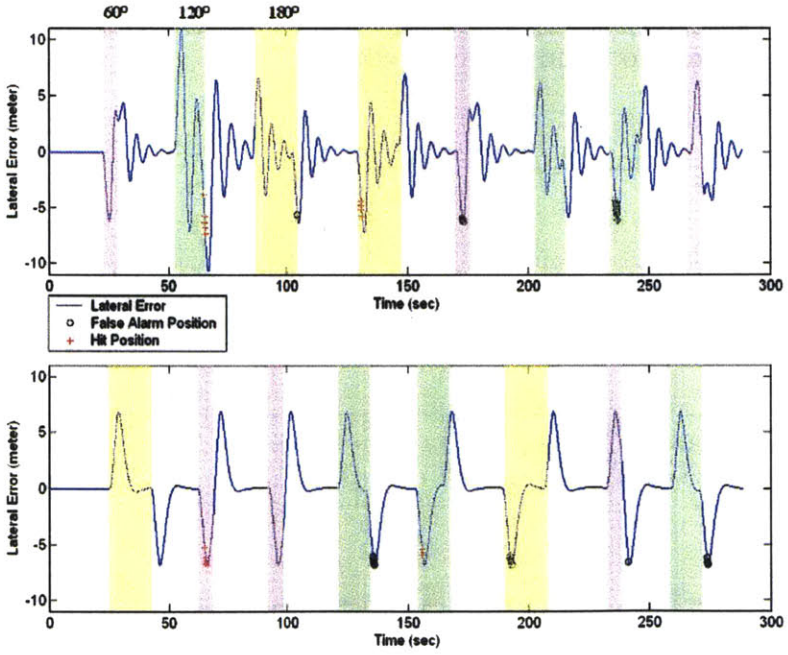

Figure 5-9: Positions of Interventions in Scenario 3 (Top) and 4 (Bottom)

According to the Figure 5-10, when humans made correct decisions, velocities

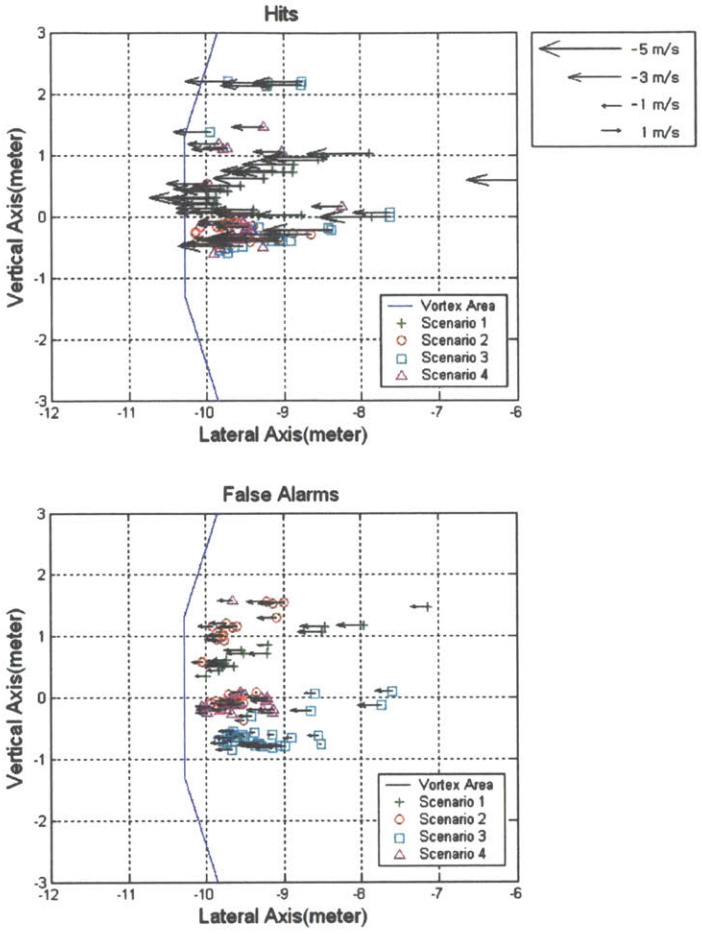

Figure 5-10: Velocity of Hits (Top) and False Alarms (Bottom)

of the wing tip was generally higher than for false alarms. There was a significant difference of velocities between hits and false alarms ($z = 9.878$, $p < 0.000$). It was observed that most false alarm interventions had negative velocities, which means the wing tip was moving toward the outside of the vortex area.

Chapter 6

Discussion

This chapter discusses the results described in Chapter 5 in detail and also examines the hypotheses proposed in Chapter 4. This chapter consists of two main areas: human's intervention performance during the display-monitoring and trust in the AFF system.

6.1 Intervention Performance

Misses

The first performance metric examined was the number of misses for each experimental scenario and as presented earlier, four experimental scenarios were provided. Scenario 1 represented the formation flight where turns were triggered by 15° angle of bank and station keeping was controlled by the oscillating controller (0.1 damping ratio). Scenario 2 was combination of turns at 15° angle of bank and the smoothing controller (0.7 damping ratio). Turns in both scenario 3 and 4 were generated by 25° angle of bank, but the oscillating controller was used in scenario 3 and the smoothing controller in scenario 4.

Among the four decisions made by the pilot, which are misses, hits, false alarms and correct rejections, misses are the most crucial decisions within the framework of safety because missing interventions in the face of extreme situations significantly threatens safety of the AFF system.

The result of this investigation by the Friedman test suggests the previous hypothesis that there is a significant difference of the number of misses between factor levels i.e. operational parameters, is correct. The subjects performed less misses with the smoothing controller when the AFF banked at 15°. Level turns with a low angle of bank during the AFF moderately introduced the heading angle rate and the smoothing controller corrected back the position of the wing tip to the reference without oscillation. In this respect, the human correctly detects through the display how dynamically the AFF turns and how oscillating the wing tip is by the controller. This implies the human's intervention accuracy can be improved at the low angle of bank and with the smoothing controller.

False Alarms

In a similar way to misses, Friedman test and post-hoc pairwise comparisons were carried out to examine the effect of the factor levels on the number of false alarms. Subjects executed the most false alarms in scenario 3 where the AFF was operated with the oscillating controller and the bank angle was allowed to 25° (Figure 5-2). This result suggests that decision-makers are less trusting when the angle of bank is high and the position that they are observing oscillates. Operators perceive that an oscillating controller is more unstable and the 25° angle of bank generates more dynamic turns.

Subject interventions appearted to have the same tendency under both correct and incorrect decisions. From the wing tip positions at the moment of interventions, it is inferred how human operators built the decision-rules in their mental model. Early interventions in scenarios 1 and 3 were executed because of oscillation of the cross, and the low trust level in the AFF system. On the contrary, in scenarios 2 and 4, the smoothing controller seems to be stable and comfortable so the human is able to wait longer to execute the interventions. That means the smoothing controller increases the trust level in the AFF system, however, sometimes incorrectly.

Poor Performance

Poor performances includes both incorrect decisions: misses and false alarms. In order to understand the human's comprehensive intervention performance, it is worth studying the effect of factors on the poor performance. As done in the analysis of misses and false alarms above, the Friedman test and Friedman multiple pairwise tests were applied. In scenario 3, the participants exhibited the poorest performances, which is similar to the result from the analysis of false alarms. It is likely that the false alarm counts dominated the poor performance metric.

The decision-makers tended to be disturbed by sharp turns generated by the high bank angle, but the levels of oscillation did not comprehensively influence on the decision-making to intervene the AFF system. Because the display was designed with 3D vortex tunnels created by the leading aircraft, the pilot in the trailing aircraft is able to perceive how sharply the AFF turns in the current and future state. Observing the leading aircraft in a high bank angle, subjects were conservative, which frequently triggered unnecessary interventions.

6.2 Decision Heuristics

Among the four types of decisions during the display monitoring, interventions included hits and false alarms: hits imply necessary interventions, and false alarms are unnecessary ones. Locations of the wing tip at the moment of interventions were measured because these locations conveyed information about how early or late the human executed the interventions in the AFF system. As long as the wing tip predictably stays inside the vortex area, the human can rely upon the automation. When the wing tip was close to the boundary of the vortex area or was on the verge of passing out of the boundary, the human tended to execute the interventions. From the graphical representation of locations of the wing tip in Figure 5-6 and 5-7, it appeared that subjects, as trailing aircraft pilots, intervened with the AFF system only when the wing tip approached the left boundary of the vortex area. Regardless of correctness of the decisions and scenarios, most interventions occurred at a specific location.

Subjects appeared to form their own decision rules during the interaction with the AFF system, which means they had a mental threshold to decide to intervene. In hits, 100 hits out of total 110 hits occured between the vortex boundary and 83.5% of radial distance from the origin. Similarly, 94 false alarms out of total 105 false alarms were made between the vortex boundary and 84.5% of radial distance from the origin (Figure 6-1). This result supports the post-hoc anaysis that subjects had indistinguishable thresholds for interventions in both hits and false alarms. In addition to the graphical representation, mean percentages of radial distances of hits and false alarms were compared to examine the difference statistically. They were found to be not significantly different when α is 0.05 ($z = 0.7560$, $p = 0.225$). In conclusion, regardless of decision accuracy, positions of interventions were the same. Figure 6-1 shows locations of interventions and a threshold that is estabilished in their mental model.

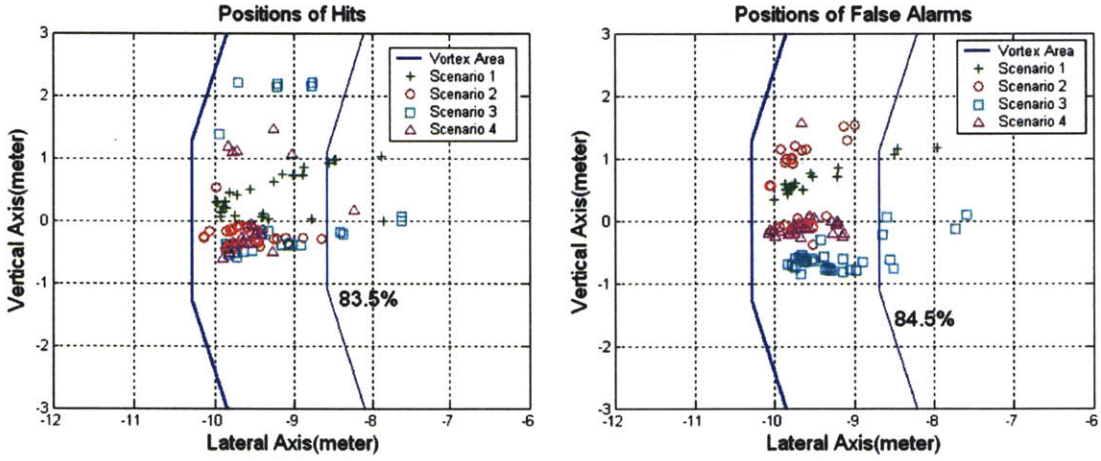

Figure 6-1: Position of Interventions and Mental Threshold

In section 5.3, it was obvious that velocities of the wing tip were significantly different between hits and false alarms. This fact demonstrates that subjects were unable to observe the velocity of the wing tip while monitoring the station-keeping display. One reason to provide velocity feedback to human operators is that human operators are not manually flying but monitoring the system in the context of human supervisory control. In order to obtain the velocity feedback of the wing tip in

the display, subjects needed to derive velocity from the moving cross with respect to the moving vortex tunnel. However, subjects interacted with the AFF system intermittently as a supervisor, so they monitored the display discretely. This occurred because of the secondary task, which was checking the distance between the leading and trailing aircraft. Because of the secondary task, the subjects could not fixate their eyes on the station-keeping display during the flight. By simultaneously monitoring the display and checking the distance, humans appeared to make decisions to intervene based on the positions of the wing tip under the time-critical situation. Therefore, humans failed to obtain the velocity feedback from the display. Figure 6-2 indicates the phase plane plots of both hits and false alarms.

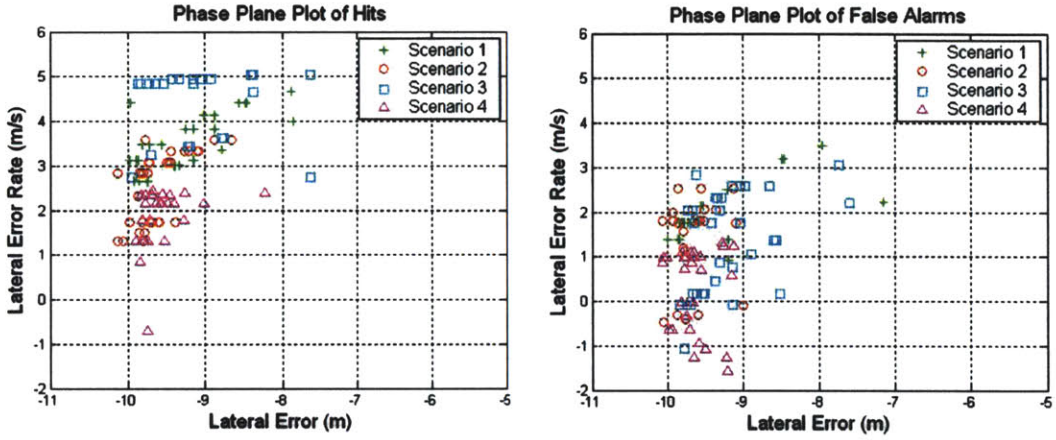

Figure 6-2: Phase plane plots of hits (Left) and false alarms (Right)

In this phase plane plot, lateral error and later error rate of the wing tip were represented in both interventions. As mentioned previously, positions of the wing tip at interventions did not show a large difference while velocities of the wing tip across two interventions were significantly different. When subjects made false alarms, magnitude of the wing tip velocity was remarkably low, indicating that the system was correcting but this was not effectively communicated to the operator. Based on the experimental results, Figure 6-3 shows the decision-making process to intervene in the AFF system.

The blue arrow shows the typical process when humans normally observe the po-

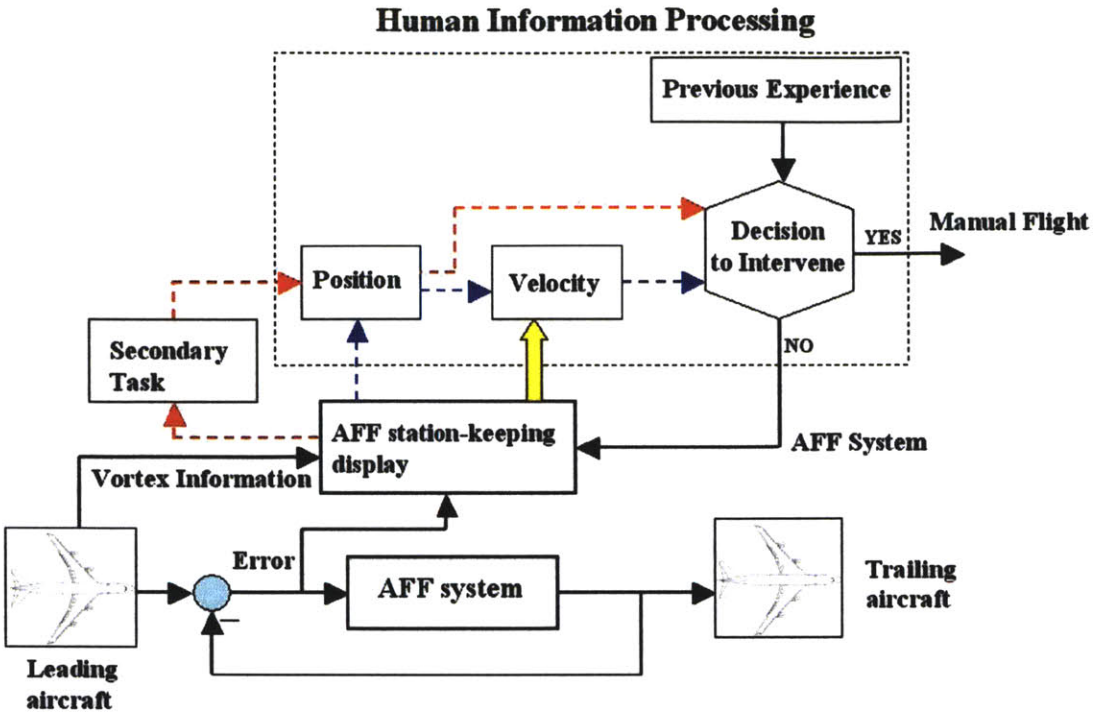

Figure 6-3: Decision-making process to intervene with the AFF system

sition and velocity of the wing tip. Once positions and velocities of the wing tip are observed on the display, humans make decisions to intervene based on their mental models. Mental models, a individual human's mental understanding of how a system works, guide interaction with the system. Mental models are not necessarily accurate and will be constrained by the user's knowledge background, previous experience with similar systems and operational conditions during interactions with systems. A mental model of functionality of the AFF system was formulated through the practice scenario which was provided before the experimental scenarios. Monitoring the practice scenario, subjects recognized how the AFF system works for keeping-station. During the practice scenario, subjects developed their own heuristics to execute interventions. Comparing the heuristics with the observed information, subjects determined whether or not they should execute interventions. However, when the secondary task was included in the monitoring task, subjects appeared to skip the need for velocity information and move directly to the decision point. The red arrows in Figure 6-3

shows this process.

In this display design, velocity, represented by a yellow block arrow, was not provided explicitly so humans needed to cognitively derive the velocity. This emphasizes that the display as designed may not be helpful to support decision-making because it provided prediction and velocity feedback with pictorial realism. However, the human operator cannot monitor continuously so discrete monitoring of the display did not help to obtain the velocity feedback. In this respect, the magnitude of the velocity is required to be shown explicitly with the position of the wing tip. This experiment shows that the velocity feedback through the motions of the vortex area and the cross appears to be ineffective even with a naturalistic display. Thus, a display with the velocity vector should be equally effective in human's performance.

Chapter 7

Conclusion

This chapter provides a summary of the experiments and presents the main findings from the study. Recommendations for future works are also included.

7.1 Overview of Study

As automation technologies advance, machines are replacing humans by performing functions that have been performed only by humans. Thus, humans supervise an automatic system by intervening with the system intermittently. One human-machine system of the future in the aeronautic field is autonomous formation flight because it reduces operating costs by decreasing fuel consumption. This technology also has a variety of applications from cargo aircraft to UAVs. Because humans cannot perform manual formation flight for a long time, humans are needed as system supervisors.

This study attempted to answer questions as to how human operators correctly intervened with an AFF system and what information influences human operators during monitoring of the station-keeping display. This study attempted to discover what operational conditions minimize incorrect decisions and how they affect the human's trust level in the AFF system. As independent variables, two operational parameters were selected: the limit of the angle of bank and the damping ratio of the AFF controller. Each independent variable had two factor levels, which provided the basis for four experimental scenarios. Incorrect decisions, misses and false alarms,

were counted in each scenarios and the position and the velocity of the wing tip were measured when subjects intervened with the AFF system. 20 subjects participated in this study.

7.2 Summary of Findings

In the analysis of intervention performances, subjects made the most incorrect interventions when the AFF was operated with the oscillating controller and high angle of bank. This was seen commonly in the study of misses, false alarms and poor performances. Because the high angle of bank generated sharp turns and the low damping ratio controller corrected the wing tip with high oscillation, two objects, the vortex area and the wing tip, were moving and required more cognitive processes to make decisions. The angle of bank had the strongest effect on poor performances rather than the damping ration of the controller.

One aspect of trust in the AFF system was investigated and this study showed that there exists an effect of damping ratio on trust of humans in the AFF system. When the AFF controller had high damping ratio and the cross moved smoothly, humans tended to intervene late and waited a longer time. This means the human mentally had a larger buffer zone in which to execute the interventions and the smoothing controller seemed to increase the trust level in the AFF system.

One of the main findings in this research is that humans developed biased decision rules when execute interventions while monitoring the AFF station-keeping display because velocity feedback was not adequately provided. The decision criteria were indistinguishable between incorrect and correct decisions, and it appeared that humans developed a mental threshold to intervene based on the position of the wing tip. Subjects sometimes failed to obtain the velocity feedback from the display, because they were out of the control loop and intermittently intervened with the automated system because they could not continuously monitor one display. An explicit velocity vector needs to be displayed to improve the human's intervention performance.

7.3 Recommendations for Future Works

Followings are recommendations for future works.

- This study just utilized a three-dimensional display for experiments and did not attempt to compare the effectiveness between different types of displays. Therefore, extension to the study of a two-dimensional display is required in future work.

- In the display used in this study, the position of the wing tip was given and a velocity vector was not included. The results showed that pictorial realism of the display did not support velocity feedback. As discussed earlier, under intermittent human supervisory control, velocity feedback from the display was difficult to obtain. A newly designed display should provide the velocity vector explicitly and the experiments should be extended to measure the effectiveness of the new display.

- The ultimate goal of the AFF is to reduce the operation cost by using aerodynamic benefits. It will be valuable to research the cost of the incorrect interventions, which are defined by misses and false alarms. They negates the benefits from fuel savings so the cost analysis of incorrect interventions will help to build the cost optimization function for the AFF system. The cost of the AFF system could be a dependent variable to evaluate the effectiveness of display.

Appendix A

Statistical Methods

A.1 ANOVA (Analysis of Variance)

The basic model in the ANOVA for the percentage of the radial distance of the wing tip is shown by the following equation.

$$y_{ijk} = \mu + \alpha_i + \beta_j + \alpha\beta_{ij} + \epsilon_{ijk} \tag{A.1}$$

y_{ijk} is the percentage of the radial distance of the wing tip when the *kth* subject underwent the AFF from the angle of bank group i and the damping ratio group j. μ is the common effect, α_i is the effect of the *ith* angle of bank, and β_j is the effect of the *jth* damping ratio. $\alpha\beta_{ij}$ is the interaction between factors α and β, and ϵ_{ijk} is the uncontrolled variation for this specific subject. In this experiment, α_i and β_j are fixed effects. The first null hypothesis is that the effects of two bank angles were the same.

$$H_{0_1} : \alpha_1 = \alpha_2 \tag{A.2}$$

The second hull hypothesis is that the effects of two damping ratios were the same.

$$H_{0_1} : \beta_1 = \beta_2 \tag{A.3}$$

The main interest is to show that these null hypotheses can be rejected at a significant confidence level. For the two factor ANOVA test, the following sum of squares (SS), mean squares (MS), degrees of freedoms (DF) and computed F ($\hat{F}$) needed to be calculated.

Source	SS	DF	MS
α	$SS\alpha = \frac{\sum_{i=1}^{a} \alpha_i^2}{bn} - \frac{\left(\sum_{i=1}^{a}\sum_{j=1}^{b}\sum_{k=1}^{n} y_{ijk}\right)^2}{abn}$	a–1	$MS\alpha = \frac{SS\alpha}{DF}$
β	$SS\alpha = \frac{\sum_{j=1}^{b} \beta_j^2}{an} - \frac{\left(\sum_{i=1}^{a}\sum_{j=1}^{b}\sum_{k=1}^{n} y_{ijk}\right)^2}{abn}$	b–1	$MS\beta = \frac{SS\beta}{DF}$
$\alpha\beta$	$SS\alpha\beta = \frac{\sum_{i=1}^{a}\sum_{j=1}^{b} \alpha\beta_{ij}^2}{n} - \frac{\sum_{i=1}^{a} \alpha_i^2}{bn} - \frac{\sum_{j=1}^{b} \beta_j^2}{an} + \frac{\left(\sum_{i=1}^{a}\sum_{j=1}^{b}\sum_{k=1}^{n} y_{ijk}\right)^2}{abn}$	(a–1)(b–1)	$MS\alpha\beta = \frac{SS\alpha\beta}{DF}$
Error	$SSE = (SST - SS\alpha - SS\beta - SS\alpha\beta)$	ab(n–1)	$MSE = \frac{SSE}{DF}$
Total	$SST = \sum_{i=1}^{a}\sum_{j=1}^{b}\sum_{k=1}^{n} y_{ijk}^2 - \frac{\left(\sum_{i=1}^{a}\sum_{j=1}^{b}\sum_{k=1}^{n} y_{ijk}\right)^2}{abn}$	abn–1	

Table A.1: ANOVA table for two factor factorial model with n replications of each combination. n=1, a=2 and b=2 for this experimnet

With the above calculation, the test statistic could be found for each effect and interaction.

$$\hat{F} = \frac{MS\alpha}{MSE} \tag{A.4}$$

$$\hat{F} = \frac{MS\beta}{MSE} \tag{A.5}$$

$$\hat{F} = \frac{MS\alpha\beta}{MSE} \tag{A.6}$$

The ANOVA calculations were done for hits and false alarms using SPSS and shown in following figures.

Tests of Between-Subjects Effects

Dependent Variable: DISTANCE

Source	Type III Sum of Squares	df	Mean Square	F	Sig.
Corrected Model	628.081[a]	3	209.360	6.298	.001
Intercept	911301.316	1	911301.316	27414.220	.000
AOB	54.295	1	54.295	1.633	.204
DAMPING	552.169	1	552.169	16.611	.000
AOB * DAMPING	23.781	1	23.781	.715	.400
Error	3556.885	107	33.242		
Total	930122.300	111			
Corrected Total	4184.967	110			

a. R Squared = .150 (Adjusted R Squared = .126)

Figure A-1: ANOVA table of percentage of distance in hits

Tests of Between-Subjects Effects

Dependent Variable: DISTANCE

Source	Type III Sum of Squares	df	Mean Square	F	Sig.
Corrected Model	283.717[a]	2	141.858	5.175	.008
Intercept	614200.607	1	614200.607	22405.917	.000
AOB	6.820	1	6.820	.249	.619
DAMPING	134.392	1	134.392	4.903	.030
AOB * DAMPING	.000	0	.	.	.
Error	1973.695	72	27.412		
Total	626211.340	75			
Corrected Total	2257.411	74			

a. R Squared = .126 (Adjusted R Squared = .101)

Figure A-2: ANOVA table of percentage of distance in false alarms

A.2 Friedman Test

Friedman (1973) has provided a test statistic $\hat{\chi}_R^2$ to test the null hypothesis that there is no treatment effect in a randomized block design with k treatments and n blocks, or simply , the k columns originated in the same population [21]:

$$\hat{\chi}_R^2 = \left[\frac{12}{nk(k+1)}\sum_{i=1}^{k} R_i^2\right] - 3n(k+1) \tag{A.7}$$

where n is of rows (individuals, replications, sample groups, blocks) and k is the number of columns (conditions, treatments, types, factors). The test statistic $\hat{\chi}_R^2$ is distributed like χ^2 for k–1 degrees of freedom if the samples are not too small. Ties within a row (i.e., equal data or mean ranks) are, strictly speaking, not allowed; the computation then follows Victor (1972):

$$\hat{\chi}_{R,T}^2 = \left\{n/\left[n - \frac{1}{k^3-k}\left(\sum_{i=1}^{n}\sum_{j=1}^{r_i}(t_{ij}^3 - t_{ij})\right)\right]\right\}\hat{\chi}_R^2 \tag{A.8}$$

with r_i the number of ties within the ith row of the ith block and t_{ij} the multiplicity of the jth tie in the ith block.

Form this statistic and degree of freedom, it is conclude whether there are considerable differences among treatments. Following figures show the computation by SPSS.

Test Statistics[a]

N	20
Chi-Square	9.111
df	3
Asymp. Sig.	.028

a. Friedman Test

Test Statistics[a]

N	20
Chi-Square	8.718
df	3
Asymp. Sig.	.033

a. Friedman Test

Figure A-3: Table of Friedman test in hits (left) and false alarms (right)

Bibliography

[1] W. Blake. Drag reduction from formation flight. Technical Report OH VA–02–02, Air Force Research Laboratory, Wright Patterson, Dec. 2002.

[2] W. Blake and D. Multhopp. Design, performance and modeling considerations for close formation flight. In *AIAA Guidance, Navigation, and Control Conference Proceedings*, Reston, VA, Jul. 2004.

[3] Jovan D. Bošković, Sai-Ming Li, and Raman K. Mehra. Formation flight control design in the presence of unknown leader commands. In *Proceedings of the American Control Conference*, Anchorage, AK, May 2002.

[4] Gene F. Franklin, J. David Powell, and Abbas Emami-Naeini. *Feedback Control of Dynamic Systems.* Addison–Wesley Publishing Company, Inc., Stanford, CA, 3rd edition edition, 1994.

[5] Dedre Gentner and Albert L. Stevens. *Mental Models.* Lawrence Erlbaum Associates, Hillsdale, NJ, 1983.

[6] F. Giulietti, L. Pollini, and M. Innocenti. Autonomous formation flight. *IEEE Control Systems*, 20(6):34–44, 2000.

[7] James K. Hall and M. Pachter. Formation maneuvers in three dimensions. In *Proceedings of the 39th IEEE Conference on Decision and Control*, Sydney, Australia, Dec. 2000.

[8] C. E. Hanson, J. Ryan, M. J. Allen, and S. R. Jacobson. Overview of flight test results for a formation flight autopilot. Technical Report NASA/TM–2002–210729, NASA Dryden, Edwards, CA, Aug. 2002.

[9] David Heeger. Singal detection theory. Technical report, Department of Psychology, New York University, Nov. 1997.

[10] D. Hummel. The use of aircraft wakes to achieve power reduction in formation flight. In *Proceedings of Fluid Dynamics Panel Symposium, AGARD*, pages 1777–1794, Nov. 1996.

[11] John Lee and Neville Moray. Trust control strategies and allocation of function in human-machine systems. *Ergonomics*, 35(10):1243–1270, Oct. 1992.

[12] B. M. Muir. Trust between humans and machines, and the design of decision aides. *International Journal of Man-Machine Studies*, 27:527–539, 1987.

[13] Bonnie M. Muir and Neville Moray. Trust in automation. part ii. experimental studies of trust and human intervention in a process control simulation. *Ergonomics*, 39(3), 1996.

[14] M. Pachter, J.J. D'Azzo, and J.L. Dargan. Automatic formation flight control. *Journal of Guidance, Control, and Dynamics*, 17(6):1380–1383, May 1994.

[15] M. Pachter, J.J. D'Azzo, and A.W. Proud. Tight formation flight control. *Journal of Guidance, Control, and Daymaics*, 24(2), Mar.–Apr. 2001.

[16] M. Pachter, Andrew W. Proud, and J.J. D'Azzo. Close formation flight control. In *Proceedings of the 1999 AIAA Guidance, Navigation and Control Conference*, Portland, OR, Aug. 1999.

[17] R. Parasuraman and V. Riley. Humans and automation: use, misuse, disuse, abuse. *Human Factors: The Journal of the Human Factors and Ergonomics Society*, 39(2):230–253, 1997.

[18] S. Park, J. Deyst, and J. How. A new nonlinear guidance logic for trajectory tracking. In *Proceedings of AIAA Guidance, Navigation, and Control Conference*, Providence, RI, Aug. 2004.

[19] L Prandtl. Induced drag of multiplanes. *National Advisory Committe for Aeronautics–Technical Notes*, (no. 182), Mar. 1924.

[20] Ronald J. Ray, Brent R. Cobleigh, M. Jake Vachon, and Clinton St. John. Flight test technigues used to evaluate performance benefits during formation flight. Technical Report NASA/TP–2002–210730, NASA Dryden, Edwards, CA, Aug. 2002.

[21] Lothar Sachs. *Applied Statistics: A Handbook of Techniques.* Springer–Verlag New York Inc., New York, NY, fifth edition, 1982.

[22] Jeffrey A. Scott. *V-Formation Flight of Birds.* Aerospaceweb.org, Jul. 2005. http://www.aerospaceweb.org/question/nature/q0237.shtml.

[23] Thomas B. Sheridan. *Telerobotics, Automation and Human Supervisory Control.* The MIT Press, Cambridge, MA, 1992.

[24] Thomas B. Sheridan. *Humans and Automation: System Design and Research Issues.* Wiley Series in System Engineering and Management. A John Wiley and Sons, Inc., Santa Monica, CA, first edition, 2002.

[25] S. N. Singh and Pachter. Adaptive feedback linearing nonlinear close formation control of uavs. In *Proceedings of the American Control Conference*, Chicago, IL, 2000.

[26] J.R. Spreiter and A.H. Sacks. Rolling up of trailing vortex sheet and its effect on downwash behind wings. *Journal of the Aeronautical Sciences*, 18(1):21–32, Jan. 1951.

[27] M. J. Vachon, R. J. Ray, K. R. Walsh, and K. Ennix. F/A–18 performance benefits measured during the autonomous formation flight project. Technical Report NASA/TM–2003–210734, NASA Dryden, Edwards, CA, Sep. 2003.

[28] H. Weimerskirch, J. Martin, Y. Clerquin, P. Alexandre, and S. Jiraskova. Energy saving in flight formation. *Nature*, 413(6857):697–698, 2001.

[29] Shoshana Zuboff. *In the Age of the Smart Machine: The Future of Work and Power.* Basic Books, New York, NY, 1988.